

# Beyond maps: Patterns of formation processes at the Middle Pleistocene open-air site of Marathousa 1, Megalopolis Basin, Greece

D. Giusti<sup>a,\*</sup>, V. Tourloukis<sup>a</sup>, G. E. Konidaris<sup>a</sup>, N. Thompson<sup>a</sup>, P. Karkanas<sup>b</sup>, E. Panagopoulou<sup>c</sup>, K. Harvati<sup>a</sup>

<sup>a</sup>*Paläoanthropologie, Senckenberg Centre for Human Evolution and Palaeoenvironment, Eberhard Karls Universität Tübingen, Rümelinstr. 23, 72070 Tübingen, Germany*

<sup>b</sup>*Malcolm H. Wiener Laboratory for Archaeological Science, American School of Classical Studies at Athens, Greece*

<sup>c</sup>*Ephoreia of Palaeoanthropology-Speleology of Greece, Athens, Greece*

---

## Abstract

Recent excavations at the Middle Pleistocene open-air site of Marathousa 1 have unearthed in one of the two investigated areas (Area A) a partial skeleton of a single individual of *Palaeoloxodon antiquus* and other faunal remains in spatial and stratigraphic association with lithic artefacts. In Area B, a much higher number of lithic artefacts was collected, spatially and stratigraphically associated also with faunal remains. The two areas are stratigraphically correlated, the main fossiliferous layers representing an *en masse* depositional process in a lake margin context. Evidence of butchering (cut-marks) has been identified on bones of the elephant skeleton, as well on elephant and other mammal bones from Area B. However, due to the secondary deposition of the main find-bearing units, it is of primary importance to evaluate the degree and reliability of the spatial association of the lithic artefacts with the faunal remains. Indeed, spatial association does not necessarily imply causation, since natural syn- and post-depositional processes may equally produce spatial association. Assessing the degree and extent of post-depositional reworking processes is crucial to fully comprehend the archaeological record, and therefore to reliably interpret past human behaviours. The present study uses a comprehensive set of spatial statistics in order to disentangle the depositional processes behind the distribution of the archaeological and palaeontological record at Marathousa 1. Preliminary results of our analyses suggest minor reworking and substantial spatial association of the lithic and faunal assemblages, supporting the current interpretation of Marathousa 1 as a butchering site.

**Keywords:** Spatial analysis, Site formation processes, Vertical distribution, Fabric analysis, Point pattern analysis, Middle Pleistocene

---

\*Corresponding author

Email address: domenico.giusti@uni-tuebingen.de (D. Giusti)

1      **1. Introduction**

2      Archaeological site formation processes, intensively studied since the early 1970s  
3    (Isaac, 1967; Schiffer, 1972, 1983, 1987; Shackley, 1978; Wood and Johnson, 1978;  
4    Binford, 1981; Schick, 1984, 1986, 1987; Petraglia and Nash, 1987; Petraglia and  
5    Potts, 1994, among others), “still insufficiently taken in consideration” (Texier, 2000,  
6    p.379) at the beginning of the 21st century, are nowadays fully acknowledged in the ar-  
7    chaeological practice (Villa, 2004; Bailey, 2007; Brantingham et al., 2007; Malinsky-  
8    Buller et al., 2011; Vaquero et al., 2012; Bargalló et al., 2016, among others). Drawing  
9    inferences about past human behaviours from scatters of archaeological remains must  
10   account for syn- and post-depositional contextual processes.

11     Several methods are currently applied in order to qualify and quantify the type and  
12   degree of reworking of archaeological assemblages. Within the framework of a geoar-  
13   chaeological and taphonomic approach, spatial statistics offer meaningful contributions  
14   in unravelling site formation and modification processes from spatial patterns. How-  
15   ever, while the spatio-temporal dimension is an ineluctable inherent property of any  
16   biotic and abiotic process, spatial statistics are still insufficiently applied.

17     Distribution maps are cornerstones of the archaeological documentation process  
18   and are primary analytic tools. However, their visual interpretation is prone to subjec-  
19   tivity and is not reproducible (Bevan et al., 2013). Since the early 1970’s (see Hodder  
20   and Orton (1976); Orton (1982) and references therein), the traditional, intuitive, ‘eye-  
21   balling’ method of spotting spatial patterns has been abandoned in favour of more ob-  
22   jective approaches, extensively borrowed from other fields. Nevertheless, quantitative  
23   methods, while still percolating in the archaeological sciences from neighbouring dis-  
24   ciplines, are not extensively used. Moreover, only a relatively small number of studies  
25   have explicitly applied spatial point pattern analysis or geostatistics to the study of site  
26   formation and modification processes (Lenoble et al., 2008; Domínguez-Rodrigo et al.,  
27   2014b,a, 2017; Carrer, 2015; Giusti and Arzarello, 2016; Organista et al., 2017, but see  
28   Hivernel and Hodder (1984) for an earlier work on the subject).

29     The goal of a taphonomic approach to spatial analysis is to move beyond distri-  
30   bution maps by applying a comprehensive set of multiscale and multivariate spatial  
31   statistics in order to reliably construct inferences from spatial patterns. An exhaustive  
32   spatial analytic approach to archaeological inference, combined with a taphonomic  
33   perspective, is essential for evaluating the depositional processes and integrity of the  
34   archaeological assemblage, and consequently for a reliable interpretation of past hu-  
35   man behaviours.

36     The present study uses a comprehensive set of spatial statistics in order to disentan-  
37   gle the depositional processes behind the spatial distribution of the archaeological and  
38   palaeontological record recovered during excavation at the Middle Pleistocene open-air  
39   site of Marathousa 1, Megalopolis, Greece (Panagopoulou et al., 2015; Harvati et al.,  
40   2016).

41      **1.1. Marathousa 1**

42     The site (Fig. 1), discovered in 2013 at the edge of an active lignite quarry, is  
43   located between two lignite seams in the Pleistocene deposits of the Megalopolis basin,  
44   Marathousa Member of the Choremi Formation (van Vugt et al., 2000). The regular

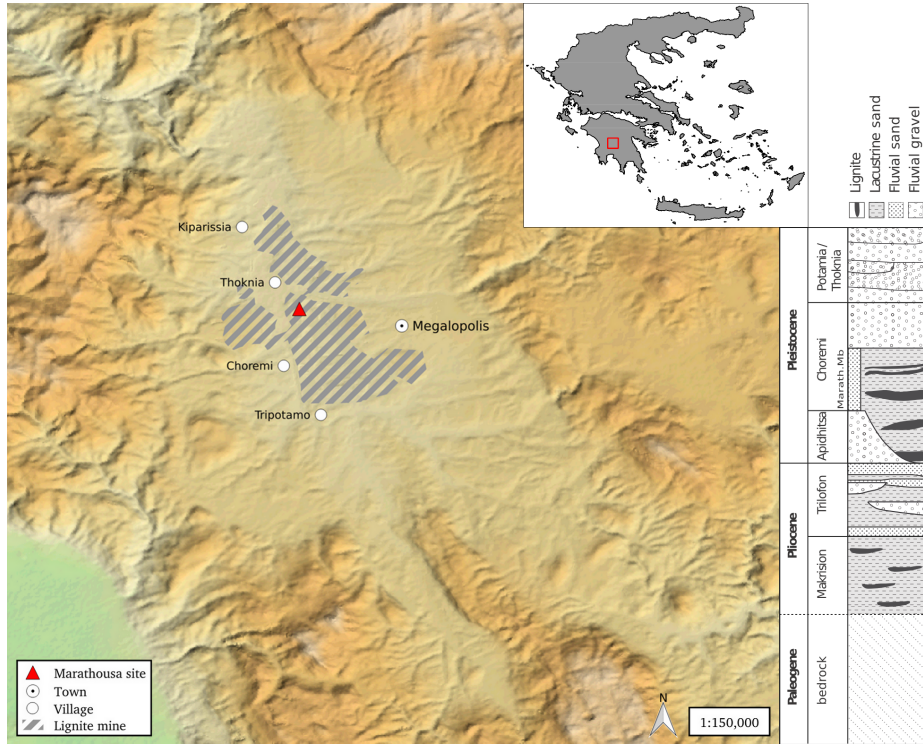


Figure 1: Geographical location of the Marathousa 1 site in the Megalopolis basin and stratigraphic column of the basin, modified after [van Vugt et al. \(2000\)](#).

45 alternation of lacustrine clay, silt and sand beds with lignite seams has been interpreted  
 46 having cyclic glacial (or stadial) and interglacial (or interstadial) origin ([Nickel et al., 1996](#)). The half-graben configuration of the basin, with major subsidence along the  
 47 NW-SE trending normal faults along the eastern margin, resulted in the gentle dip of  
 48 the lake bottom at the opposite, western, margin of the lake, enabling the formation of  
 49 swamps and the accumulation of organic material for prolonged periods of time ([van  
 50 Vugt et al., 2000](#)).

51 Two excavation areas have been investigated since 2013 (Fig. 2): Area A, where  
 52 several skeletal elements of a single individual of *Palaeoloxodon antiquus* have been  
 53 unearthed, together with a number of lithic artefacts; and Area B, located 60 m to  
 54 the South along the exposed section, where the lithic assemblage is richer and occurs  
 55 in association with a faunal assemblage composed of isolated elephant bones, cervids  
 56 and carnivores among others ([Konidaris et al., this issue](#); [Tourloukis et al., this issue](#)).  
 57 Evidence of butchering (cut-marks) have been identified on two of the elephant bones  
 58 from Area A, as well on elephant and other mammal bones from Area B ([Konidaris  
 59 et al., this issue](#)).

60 The sedimentary sequence of the site (Fig. 3) includes lacustrine and fluvio-lacustrine  
 61 clastic deposits sandwiched between two lignite seams (UA7-UB10 and UA1-UB1)

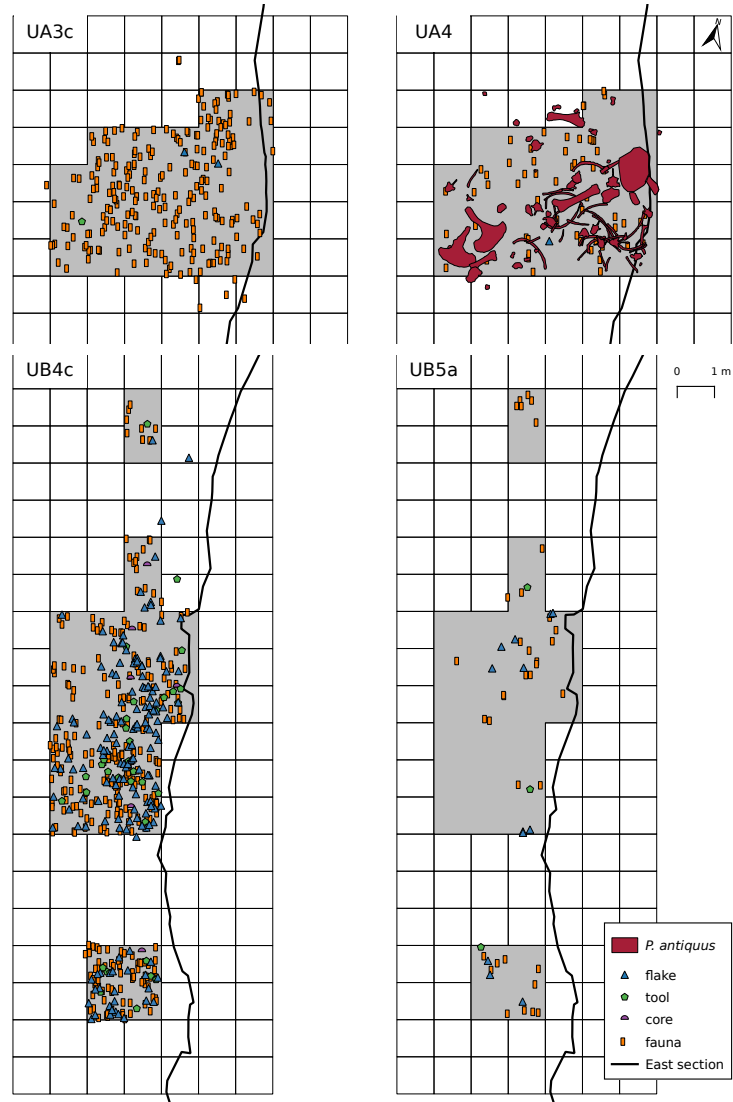


Figure 2: Distribution maps of the plotted remains from areas A (units UA3c and UA4) and B (units UB4c and UB5a). Grey zones mark the 2013-2015 excavation areas. The plotted remains of the *P. antiquus* skeleton were collected until 2016. Area B is located 60 m to the South, along the exposed East section of the lignite quarry.

(Karkanas et al., this issue). A major hiatus (contacts between UA3 and UA4, and between UB5 and UB6), attributed to exposure and erosion of a lake shore mudflat, divides the sequence in two parts. The lower part is characterised by relatively high rate sub-aqueous sedimentation of bedded sands and silts, containing low organic and carbonate content. The upper one is characterised by a series of erosional bounded depositional units, attributed to sub-aerial originated organic- and carbonate-rich mud flows and hyperconcentrated flows deposited at the margin of a swamp (Karkanas et al., this issue).

The erosional contacts UA3c/4 and UB4c/5a separate the two main find-bearing units in both areas (fig. 3). In Area A, the elephant remains lie at the contact of UA3c/4 and are covered by UA3c (Fig. 4a); while in Area B, most of the remains were collected from unit UB4c (Fig. 4b). Units UA3c and UB4c (organic- and intraclast-rich silty sands) resemble dilute mud flows, showing a chaotic structure of rip-up clasts from the underlying unit, small-to-large wood fragments and rare rock clasts. In Area B, a relatively low number of remains was also found in massive organic-rich silty sands (UB5a), which locally overlay channelised sands (UB5b/c), probably not preserved in Area A (Karkanas et al., this issue).

The flow event described above (units UA3c and UB4c), and specifically the erosional contacts between the fossiliferous horizons in the two areas (UA3c/4 and UB4c/5a), provide the essential background for the analysis and interpretation of the spatial distributions at Marathousa 1.

The secondary depositional nature of the main find horizons raises the question of how reliable is the spatial association between the lithic artefacts and the partial skeleton of a single *Palaeoloxodon antiquus* individual and other faunal remains. Since spatial association does not necessarily imply causation, and consequently synchrony, the answer has important consequences for the interpretation of the site in the broader context of the Middle Pleistocene human-proboscidean interactions. We aim to tackle this question and disentangle the formation processes acting at Marathousa 1 on the basis of spatial patterns through a three-prong spatial analytic approach:

1. by analysing, in a frame of references, the orientation patterns of remains from relevant stratigraphic units;
2. by quantifying and comparing their relative vertical distributions;
3. by identifying spatial trends in either the assemblage intensities and the associations between classes of remains.

Two contrasting models of deposition are tested: the autochthonous hypothesis (*sensu* Fernández-López, 1991; Domínguez-Rodrigo et al., 2012) states that the flow event, represented by units UA3c and UB4c, eroded and scoured the exposed surface (where the elephant was lying), thereby entraining clastic material (including artefacts) and re-depositing (*sensu* Fernández-López, 1991) this material at a close distance. This model implies the loss of any original, pristine spatial relations between remains, but minor transport from the primary depositional *loci*. On the other hand, the allochthonous hypothesis (*sensu* Fernández-López, 1991; Domínguez-Rodrigo et al., 2012) implies significant transport from the original *loci* of deposition and re-elaboration (*sensu* Fernández-López, 1991). According to this model, the spurious spatial associ-

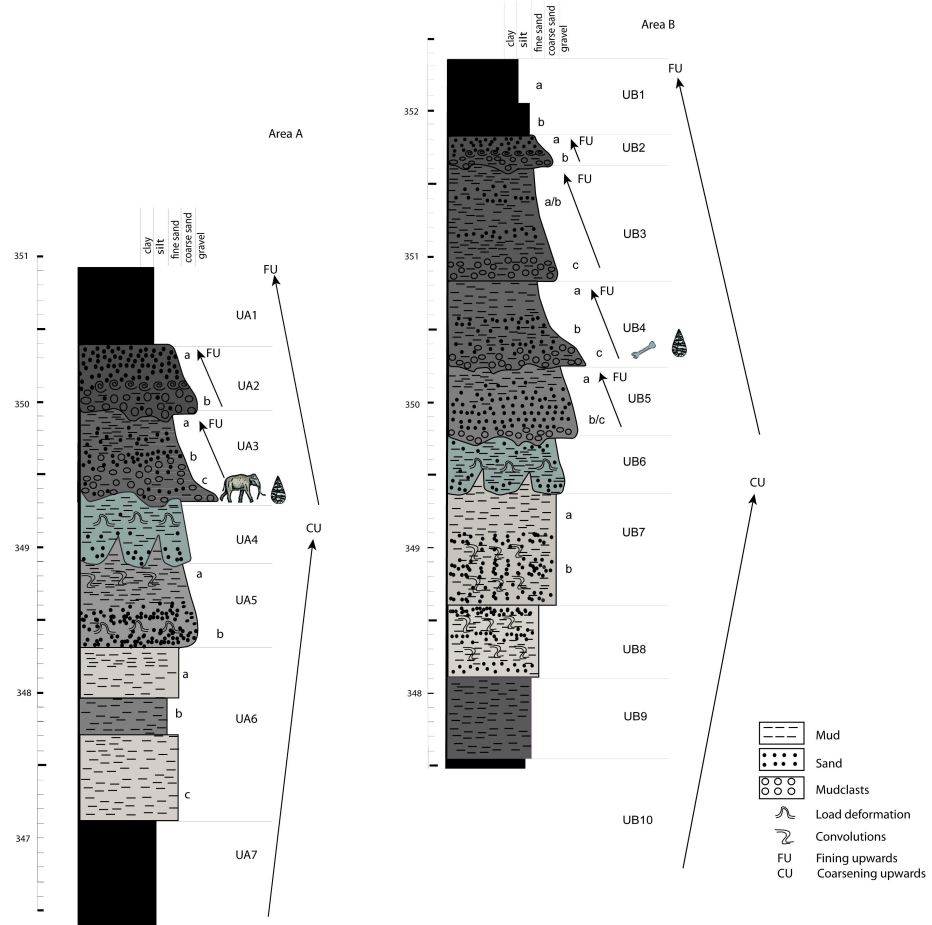


Figure 3: Stratigraphic setting of the Marathousa 1 site, modified after Karkanas et al. ([this issue](#)). Absolute elevations in m a.s.l.

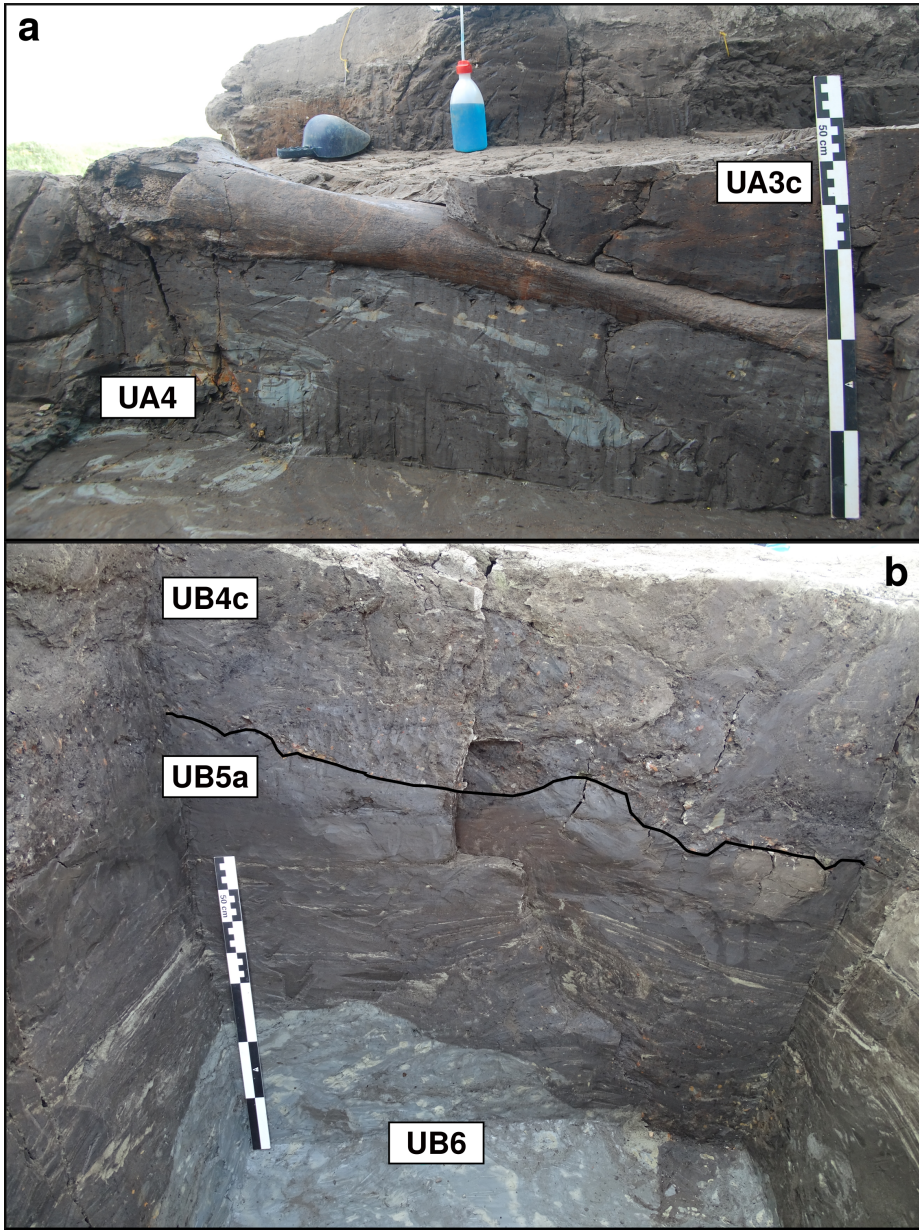


Figure 4: Photograph (2017) of the left femur of the *P. antiquus* skeleton, lying at the UA3c/4 contact and covered by unit UA3c (a). West profile (2014) of the excavation Area B (square 932/603), exposing the UB4c/5a (black solid line) and the UB5/6 erosional contacts (b).

107 ation between the lithic artefacts and faunal remains does not support any behavioural  
108 interpretation.

109 **2. Material and methods**

110 Since 2013, systematic investigation of the Marathousa 1 site has been carried out  
111 by a joint team from the Ephoreia of Palaeoanthropology-Speleology (Greek Ministry  
112 of Culture) and the University of Tübingen. A grid system of 1 square meter units  
113 was set up, oriented -14 degrees off the magnetic North, and including the two areas  
114 of investigation. The excavation of the deposit proceeded in 50x50 cm sub-squares in  
115 Area B and 1x1 m squares in Area A, and spits of 5 to 10 cm thickness, respectively.  
116 Systematic water-screening of sediments was carried out on-site using 1 mm sieves  
117 in order to guarantee recovery of the small-size fraction (e.g., micro-artefacts, small  
118 mammal remains, fish, molluscs and small fragments of organic and inorganic mate-  
119 rial). The three-dimensional coordinates of finds (i.e., all the lithic artefacts, teeth and  
120 diagnostic bones; bones and organic material with a-axis  $\geq 20$  mm), collected spits  
121 of sediment, samples and geological features (e.g., erosional contacts and mud cracks)  
122 were recorded with a total station. Dense clouds of surface points of the elephant skele-  
123 tal elements were acquired using both a total station and a close-range photogrammetric  
124 technique.

125 The dimensions (length, width and thickness) of registered finds were measured  
126 on-site with millimetre rules. Orientation (plunge and bearing) of elongated particles  
127 (i.e., faunal remains, large wood fragments and lithic artefacts) was recorded since  
128 2013 using a clock-like system (the bearing was measured, relatively to the grid North,  
129 in twelve clockwise intervals of 30°; the plunge with a 22.5° accuracy). In 2015, the  
130 use of a compass and inclinometer with an accuracy of 1° was introduced in Area B to  
131 gradually replace the former method.

132 The widespread use of a compass and inclinometer to record orientation data (Voorhies,  
133 Fiorillo, 1991; Bertran and Texier, 1995; Bertran et al., 1997; Lenoble and  
134 Bertran, 2004; Eberth et al., 2007; Eren et al., 2010; Benito-Calvo et al., 2011; Domínguez-  
135 Rodrigo et al., 2012; Domínguez-Rodrigo and García-Pérez, 2013; Domínguez-Rodrigo  
136 et al., 2014c; Cobo-Sánchez et al., 2014; Organista et al., 2017, among others) was  
137 favoured over the alternative use of a total station (Kluskens, 1990; Dibble et al., 1997;  
138 McPherron, 2005; Enloe, 2006; Bernatchez, 2010, among others), mostly due to the  
139 time-restricted conditions of the rescue excavation conducted at Marathousa 1.

140 Measurements of the bearing (azimuth) and plunge (dip) of elongated finds were  
141 taken along the symmetrical longitudinal a-axis (SLA) of bones (Domínguez-Rodrigo  
142 and García-Pérez, 2013), lithic artefacts (Bertran and Texier, 1995) and wood frag-  
143 ments (Macdonald and Jefferson, 1985), using the lowest endpoint of the a-axis as an  
144 indicator of the vector direction.

145 Other major axes have been alternatively used with the recent application of GIS  
146 techniques to retrieve orientation data from secondary source, i.e., from excavation  
147 photographs, drawings or maps (Boschian and Saccà, 2010; Benito-Calvo and de la  
148 Torre, 2011; de la Torre and Benito-Calvo, 2013; Walter and Trauth, 2013; García-  
149 Moreno et al., 2016; Sánchez-Romero et al., 2016). However, the experimental works  
150 of Domínguez-Rodrigo and García-Pérez (2013) and Domínguez-Rodrigo et al. (2014c)

151 showed that the SLA, defined as the major axis which symmetrically divide the bone,  
152 is more accurate in estimating the flow direction, regardless of bone shape. This a-axis  
153 is widely used in taphonomic studies (Toots, 1965; Voorhies, 1969; Eberth et al., 2007;  
154 Domínguez-Rodrigo et al., 2012, 2014a; Aramendi et al., 2017, among others) for de-  
155 termining the preferential orientation of anisotropic assemblages. The a-axis or major  
156 axis of the artefact, measured as the long diameter (Krumbein, 1941), is as well used  
157 in studies which employ a sedimentological approach to archaeological fabric (Bertran  
158 and Texier, 1995; Bertran et al., 1997; Lenoble and Bertran, 2004; Benito-Calvo et al.,  
159 2009, among others).

160 The present study focuses on the excavated stratigraphic units in which most of the  
161 archaeological and palaeontological remains were recovered in both excavation areas,  
162 namely in UA3c and UA4 in Area A, and UB4c and UB5a in Area B. From the total,  
163 subset samples of material were used for each specific spatial analysis. For the fabric  
164 analysis we included material collected until 2016. For the vertical distribution and  
165 point pattern analyses, the region of investigation was limited to the squares excavated  
166 from 2013 until 2015, 25 and 29 square meters respectively in each area (Fig. 2).

167 The analyses were performed in R statistical software (R Core Team, 2017). In  
168 order to make this research reproducible (Marwick, 2017; Marwick et al., 2017), a  
169 repository containing a compendium of data, source code and text is open licensed and  
170 available at the DOI: [10.5281/zenodo.1043974](https://doi.org/10.5281/zenodo.1043974)

### 171 *2.1. Fabric analysis*

172 The taphonomic study of the orientation pattern of elongated sedimentary particles,  
173 including bones and artefacts, first addressed by Voorhies (1969); Isaac (1967); Bar-  
174 Yosef and Tchernov (1972); Schick (1986), more recently led to a noteworthy develop-  
175 ment of methods and propagation of applications in Palaeolithic site formation studies  
176 (Bertran and Texier, 1995; Bertran et al., 1997; Lenoble and Bertran, 2004; Lenoble  
177 et al., 2008; McPherron, 2005; Benito-Calvo et al., 2009, 2011; Benito-Calvo and de la  
178 Torre, 2011; Bernatchez, 2010; Boschian and Saccà, 2010; Domínguez-Rodrigo et al.,  
179 2012; Domínguez-Rodrigo and García-Pérez, 2013; Domínguez-Rodrigo et al., 2014c;  
180 de la Torre and Benito-Calvo, 2013; Walter and Trauth, 2013; García-Moreno et al.,  
181 2016; Sánchez-Romero et al., 2016, among others).

182 Fabric analysis can provide valuable insight into site formation and taphonomic  
183 processes, allowing discrimination between different orientation patterns (isotropic,  
184 linear or planar) possibly associated with a range of sedimentary processes. Whereas  
185 water-flow deposits are generally characterised by relatively good sorting and preferred  
186 orientation of clasts parallel, or normal to the flow direction (linear fabric) (Petraglia  
187 and Potts, 1994); debris-flow deposits mostly exhibit massive, poorly bedded mixtures  
188 of unsorted sediments and random orientation of clasts (isotropic fabric), except at the  
189 flow margins where linear fabric may occur (Pierson, 2005). On the other hand, undis-  
190 turbed archaeological sites, as well as experimental assemblages, have been observed  
191 to have planar fabric (Bertran et al., 1997; Lenoble and Bertran, 2004). Nevertheless,  
192 grey zones exist between depositional processes, so that an unequivocal discrimination  
193 based only on fabric observations is often not possible, and other taphonomic criteria  
194 must also be considered (Lenoble and Bertran, 2004). As an example, while overland  
195 flows (runoff) have been observed to show some degree of planar fabric (Lenoble and

[Bertran, 2004](#)), anisotropy without significant transport can be caused in a lacustrine floodplain by low-energy processes such as lake transgression and regression, as well as water-sheet flows formed during rainy seasons ([Cobo-Sánchez et al., 2014](#)).

At the margin of a lacustrine environment, relatively close to the surrounding relief, a combination of high- and low-energy processes can be expected. According to the sedimentological and micromorphological study of the Marathousa 1 site, the main find-bearing horizon is associated with hyperconcentrated flows ([Karkanas et al., this issue](#)). Hyperconcentrated flows are intermediate states, defined by sediment concentration, in the continuum between sub-aerial water flows and debris flows. [Benvenuti and Martini \(2002\)](#) reported that, when a turbulent hyperconcentrated flow expands over a surface - as in the case of Marathousa 1 - a two-phase flow may develop, with a more concentrated, coarser grained bottom flow-layer (traction carpet) moving slower than the upper turbulent flow-layer carrying wash-load and suspended load. Resultant deposit may exhibit diagnostic inverse grading, or a continuously aggrading bed. Parallel or normal orientation of the clasts to the flow direction can be observed ([Benvenuti and Martini, 2002](#)). A simulation model also showed that linear fabric can develop in mud flows. However, after deposition, settling of the clasts may affect the fabric to some extent, depending on the viscosity of the mud flow ([Lindsay, 1968](#)).

As part of our three-prong spatial analytic approach, we conducted comparative fabric analysis with the aim to investigate the dynamics of the depositional processes at Marathousa 1.

Since fabric strength has been found to be positively correlated with the shape and size of the clast, for the fabric analysis we subset samples of remains with length  $\geq 2$  cm and elongation index (the ratio length/width)  $I_e \geq 1.6$  ([Lenoble and Bertran, 2004](#)). The samples are listed in Table 1 and include mostly wood fragments and faunal remains from the four stratigraphic units under investigation. Bones have been found to readily react to water flow and show very early anisotropic patterns ([Domínguez-Rodrigo et al., 2014c](#)). Flume experiments showed that wood fragments as well tend to align parallel to the current direction ([Macdonald and Jefferson, 1985](#)). No distinction of skeletal elements was made, both due to the high fragmentation rate of faunal remains in Area B, and because recent experiments showed a similar orientation pattern for different bone shapes ([Domínguez-Rodrigo et al., 2012; Domínguez-Rodrigo and García-Pérez, 2013](#)).

The sample of bones belonging to the individual of *P. antiquus* from Area A was analysed separately and included the humerus, ulna, femur and tibia; the atlas, axis and other 16 complete vertebrae or vertebral fragments; 29 complete ribs or rib fragments; 2 calcanea; 4 metatarsals/metacarpals; the pyramidal; the trapezoid and the pelvis. The sample from UB5a was too small (only 7 observations) and was therefore excluded. In order to assess the reliability of the orientation data recorded using the clock method, we separately analysed two sub-samples from unit UB4c, selected from a set of finds recorded using both methods. All the sampled observations are representative of the whole study area.

Rose diagrams and uniformity tests, such as Rayleigh, Kuiper, Watson and Rao tests ([Jammalamadaka et al., 2001](#)), were used to visualise and evaluate circular isotropy in the sample distribution. The Rayleigh test is used to assess the significance of the sample mean resultant length ( $\bar{R}$ ), assuming that the distribution is unimodal and not

Table 1: List of sampled observations for the fabric analysis.

Sample	<i>n</i>	Type		
		Fauna	Wood	Lithic
UA3c	49	23	25	1
UA4	38	8	30	-
<i>P. antiquus</i>	63			
UB4c	38	30	1	7

242 bi- or plurimodal. The  $\bar{R}$  ranges from 0 to 1: values close to 1 indicate that the data are  
 243 closely clustered around the mean direction; when the data are evenly spread  $\bar{R}$  has a  
 244 value close to 0. A *p* – *value* lower than 0.05 rejects the hypothesis of uniformity with  
 245 a 95% confidence interval. Kuiper, Watson and Rao are omnibus tests used to detect  
 246 multimodal departures from circular uniformity. The test results are evaluated against  
 247 critical values: a result higher than the critical value rejects with confidence the null  
 248 hypothesis.

249 Randomness testing of three-dimensional data was conducted with the Woodcock  
 250  $S_1/S_3$  test (Woodcock and Naylor, 1983). Considering both the plunge and bearing  
 251 of the oriented items, this method, based on three ordered eigenvalues ( $S_1, S_2, S_3$ ), is  
 252 able to discriminate the shape and strength of the distributions. The shape parameter  
 253  $K = \frac{\ln(S_1/S_2)}{\ln(S_2/S_3)}$  ranges from zero (uni-axial girdles) to infinite (uni-axial clusters). The  
 254 parameter  $C = \ln(S_1/S_3)$  expresses the strength of the preferential orientation, and  
 255 its significance is evaluated against critical values from simulated random samples of  
 256 different sizes. A perfect random uniform distribution would have  $C = 0$  and  $K = 1$ .

257 The Benn diagram (Benn, 1994) adds to the Woodcock test an isotropy ( $IS =$   
 258  $S_3/S_1$ ) and an elongation ( $ES = 1 - (S_2/S_1)$ ) index. Like the former method, it is  
 259 able to differentiate between linear (cluster), planar (girdle) or isotropic distributions.  
 260 There are no published raw data from actualistic studies on hyperconcentrated flows or  
 261 other depositional processes affecting the orientation of bones and artefacts deposited  
 262 on lacustrine floodplains (but see Morton (2004) and Cobo-Sánchez et al. (2014) as  
 263 pioneer studies on this subject). However, we included in the Benn diagram relevant  
 264 references to published results from observation of fabrics in modern subaerial slope  
 265 deposits, i.e., debris flow and runoff (Bertran et al., 1997; Lenoble and Bertran, 2004).

## 266 2.2. Vertical distribution

267 The vertical distribution of materials has been long investigated with the aim of  
 268 identifying cultural levels, by visually interpreting cross-sectional plots. However,  
 269 recent advances in GIS techniques allow to inspect at higher resolution the three-  
 270 dimensional distributions of archaeological remains (McPherron et al., 2005; Anderson  
 271 and Burke, 2008, among others).

272 In analysing the vertical dispersion of material at Marathousa 1, we provisionally  
 273 assume that a general concentration of unsorted lithic artefacts and faunal remains in  
 274 the proximity of the erosional surfaces would support an autochthonous origin of the  
 275 assemblages; whereas a homogeneous vertical distribution of remains from the UA3c  
 276 and UB4c units would suggest an allochthonous origin, significant transport and subse-

Table 2: List of sampled observations for the vertical distribution and point pattern analyses.

Sample	<i>n</i>	Lithic class					Faunal class			
		Debris/chip	Flake	Bone flake	Tool	Core	Indet.	Bone	Tooth	Microfauna
UA3c	279	46	2	-	1	-	1	171	14	44
UA4	61	3	1	-	-	-	-	45	4	8
UB4c	1243	753	154	1	34	6	2	246	28	19
UB5a	101	50	12	-	3	-	-	30	3	3

quent re-deposition of the material. Indeed, massive process such as hyperconcentrated flows, have high erosional power and rather chaotic structure, which may result in inverse or normal grading ([Benvenuti and Martini, 2002](#)).

In order to estimate the degree of vertical dispersion while controlling for the size of the archaeological material, dimensional classes were set up following typological criteria. Lithic artefacts were classified as debris/chips when smaller than a cutoff length of 15 mm ([Tourloukis et al., this issue](#)). Other classes include flakes, tools and cores; the latter being the bigger and heavier debitage product. Table 2 summarises the sample size for each class. Lithic debris/chips constitute the larger part of the assemblage from UB4c (60%) and UB5a (49%); whereas in Area A they represent only a moderate percentage in the upper UA3c unit (16%). The very rare presence of lithic artefacts in the underlying unit UA4 is nevertheless significant. In this unit, the faunal remains are also found in much lower numbers, their number reduced to one fourth of those found in UA3c. For the point pattern analysis (see below), we used the same subset of material for both excavation areas.

For Area B, the material recovered from the water-screening was randomly provenanced according to the 5 cm depth of the excavated spit and the coordinates of the 50x50 cm quadrant of the excavation square. Following the same excavation protocol, the same procedure was applied for the water-screened material of Area A, which was randomly provenanced according to 3D-coordinates of the 1x1 m excavation square and 10 cm spit.

Ordinary Kriging interpolation of the recorded points of contact between the UA3c/UA4 and the UB4c/UB5a stratigraphic units were used to reconstruct the UA3c/4 and UB4c/5a erosional surfaces (Fig. 5a,b). In geostatistics, Kriging is a method of interpolation which, from a modelled function of spatial autocorrelation between known points (e.g., recorded elevations), calculates values of unknown points (e.g., predicted elevations). Thus, in order to address our specific objective, i.e., to quantify and analyse the vertical distribution of the archaeological and palaeontological material, we measured the minimum orthogonal distance (*d*) of each specimen to the interpolated erosional surface (Fig. 5c). For the units above and below this surface (i.e., UB4c and UB5a), the relative distribution of lithic classes and faunal remains was informally tested by means of kernel density estimations.

In Area A, the UA3c/4 erosional contact is locally sharp, but, in contrast to Area B, parts of the eroded unit UA4 are mixed with pockets of the UA3c organic-rich silty sands and intraclast-rich mud flows ([Karkanas et al., this issue](#)). However, from sparse known points of the erosional contact, the UA3c/4 surface was interpolated and the vertical dispersion of remains estimated as well. The elephant remains were excluded

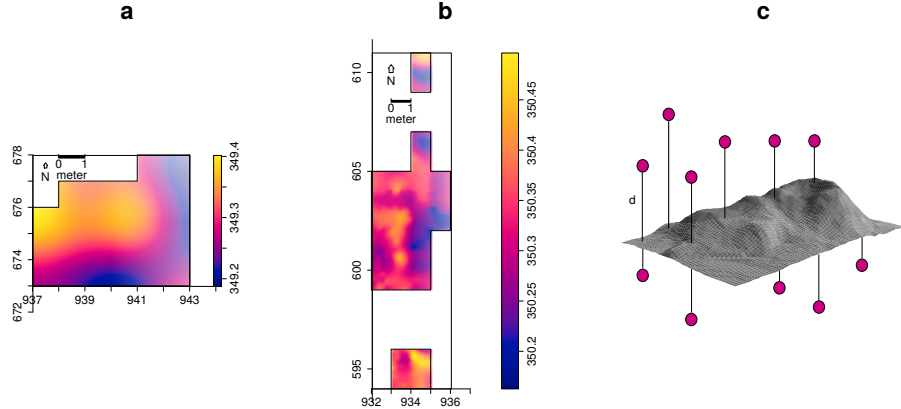


Figure 5: Ordinary Kriging interpolation of the UA3c/4 (a) and UB4c/5a (b) erosional surface; the colour scale denotes absolute elevation in m a.s.l. (c) Illustration of the method used to quantify the vertical dispersion of remains (d) with respect to the UA3c/4 (a) and UB4c/5a (b) surface.

314 from this analysis, since they clearly lie horizontally at the UA3c/4 contact (Fig. 4a).

315 Finally, a Student's two sample t-test allowed us to compare the empirical distributions  
316 of different groups of remains for each stratigraphic unit.

### 317 2.3. Point pattern analysis

318 A spatial point pattern is defined as the outcome of a random spatial point process  
319 (repetitions of it would always create a different pattern). The observed patterns of the  
320 archaeological and palaeontological remains were treated as manifestations of spatial  
321 point processes, i.e., site formation processes. Point pattern analysis investigates the  
322 spatial arrangement of points with the aim of identifying spatial trends. In order to  
323 integrate the previous studies of the fabric and vertical distributions, we directed our  
324 point pattern analysis equally to the intensity of the patterns (the rate of occurrence of  
325 the recorded finds) and to the spatial interaction between different types of finds.

326 As the average number of random points per unit area, intensity informs about  
327 homogeneity or inhomogeneity in the distribution of events (e.g., clasts) generated by  
328 a point process (e.g., mud flow), i.e., whether the rate of occurrence is uniform or  
329 spatially varying across the study area. Intensity, usually non-parametrically evaluated  
330 by means of kernel density estimation (Diggle, 1985), was assessed for the distribution  
331 of material from the UB4c, UB5a and UA3c units. Cross-validation bandwidth, which  
332 assumes a Cox process, and edge correction were applied using the methods described  
333 in Diggle (1985).

334 In the presence of a covariate, it is recommended to further investigate the dependence  
335 of intensity on that explanatory variable (Baddeley et al., 2012). In order to  
336 evaluate whether variation in the density of materials was correlated to the topography  
337 of the erosional surface, we computed a local likelihood smoothing estimate of the in-  
338 tensity of remains from UB4c as a function of the UB4c/5a surface elevation model.  
339 Formal tests enabled us to assess the evidence of that dependence and to quantify the

strength of the covariate. The Kolmogorov-Smirnov test of CSR (Complete Spatial Randomness) and Berman's  $Z_2$  statistics were used to test the strength of evidence for a covariate effect. The Receiver Operating Characteristic (ROC) plot, and the area under the ROC curve (AUC), closely related to Berman's  $Z_2$  test, measure the magnitude of the covariate effect. AUC values close to 1 or 0 indicate strong discrimination, whereas intermediate values (0.5) suggest no discrimination power.

Intensity, evaluated by means of kernel density maps, although informative and widespread in the literature, nonetheless does not provide sufficient information to reliably infer about site formation processes.

Whereas intensity is a first-order property of the point process, multiscale inter-point interaction is measured by second or higher-order moment quantities, such as the Ripley's  $K$  correlation function (Ripley, 1976, 1977) and the distance  $G$ -,  $F$ - and  $J$ -functions. Three different types of inter-point interaction are possible: random, regular or cluster. In a hypothesis-testing framework, point-wise envelopes are computed by a number of random simulations of the null hypothesis (i.e., random/Poisson distribution). Thus, values of the empirical distribution (black solid line) are plotted against the benchmark value (red dotted line) and the envelopes (grey area) which specify the critical points for a Monte Carlo test (Ripley, 1981). Regular patterns are assumed to be the result of inhibition processes, while cluster patterns are the result of attraction processes.

In order to test the spatial interaction between remains associated with the erosional event of UB4c and those associated with the underlying UB5a unit, we treated the data as a multivariate point pattern, assuming that the point patterns in UB4c and UB5a are expressions of two different stationary point processes, i.e., depositional events. We performed a cross-type pair correlation function ( $g_{ij}(r)$ ), derivative of the multitype  $K_{ij}(r)$  function, which is the expected number of points of type  $j$  lying at a distance  $r$  of a typical point of type  $i$ . The function is a multiscale measurement of the spatial dependence between types  $i$  (UB4c) and  $j$  (UB5a). Randomly shifting in 199 Monte Carlo permutations each of the two patterns, independently of each other, estimated values of  $\hat{g}_{ij}(r)$  are compared to a benchmark value  $g_{ij}(r) = 1$ , which is consistent with independence or at least with lack of correlation between the two point processes.

In addition to the pair correlation function, the multitype nearest-neighbour  $G_{ij}(r)$  function was used to estimate the cumulative distribution of the distance from a point of type  $i$  (UB4c) to the nearest point of type  $j$  (UB5a). It measures the spatial association between the two assemblages. For the cross-type  $G$ -function, the null hypothesis states that the points of type  $j$  follow a Poisson (random) distribution in addition to being independent of the points of type  $i$ .

Thus, in a randomisation technique, when the solid line of the observed distribution ( $\hat{G}_{ij}(r)$  or  $\hat{g}_{ij}$ ) is above or below the shaded grey area, the pattern is significantly consistent with clustering or segregation, respectively. In order to reduce the edge effect bias in estimating the correlation between points, we implemented Ripley's isotropic edge correction (Ohser, 1983; Ripley, 1988).

Complete spatial randomness and independence (CSRI) of the two point processes (UB4c and UB5a) would support an allochthonous origin hypothesis for the assemblage recovered from the UB4c unit. According to the allochthonous model, the massive, chaotic UB4c flow event randomly re-elaborated the material entrained in it, inde-

Table 3: Value and  $p$  – value of circular uniformity test statistics.

Sample	mean dir.	Rayleigh		Kuiper		Watson		Rao	
		R	p	V <sub>n</sub>	p	U <sup>2</sup>	p	U	p
UA3c	77.17°	0.268	0.029	2.4698	<0.01	0.2967	<0.01	271.8367	<0.001
UA4	35.79°	0.386	0.003	2.5656	<0.01	0.3437	<0.01	246.3158	<0.001
<i>P. antiquus</i>	54.64°	0.489	2.775e-07	3.4811	<0.01	0.906	<0.01	291.4286	<0.001
UB4c (clock)	91.66°	0.276	0.054	1.8963	0.01< $p$ <0.025	0.1937	0.025< $p$ <0.05	255.7895	<0.001
UB4c (compass)	151.17°	0.243	0.106	1.3944	>0.15	0.1268	>0.10	128.5263	>0.10

pendently from the material deposited in UB5a. On the other hand, positive or negative association can be interpreted as expressions of different autochthonous processes.

As for the three-dimensional distribution of the lithic artefacts in Area A, and their spatial association with the partial skeleton of the *P. antiquus*, we applied three-dimensional univariate and bivariate second-order functions. A rectangular box of 20 square meters and 80 cm vertical extent was selected for the analyses (green outline in Fig. 11a). Assuming homogeneity, the univariate pair correlation function ( $g_3(r)$ ) was estimated for the pattern of all the artefacts (mostly debris/chips) from UA3c and UA4.

In the specific context of the site, complete spatial randomness (CSR) would suggest that the pattern most probably is the result of a random distribution process, such as a high energy mass movement, thus supporting an allochthonous model of deposition. On the other hand, spatial aggregation would support a primary origin of the assemblage. Nevertheless, topography and natural obstructions may generate spatial clustering as well.

In support to the pair correlation function, the cross-type nearest-neighbour function has been applied in order to compute, for each artefact recovered from the UA3c and UA4 units, the nearest point of the three-dimensional clouds of points associated with the elephant skeleton. A prevalence of short distances would indicate aggregation of the lithic artefacts around the mass of the elephant; whereas a uniform or symmetric distribution would support the action of random independent processes

### 3. Results

#### 3.1. Fabric analysis

The rose diagrams in Fig. 6 visualise the circular distributions of the examined specimens. Overall, the UA4 sample and the sample of elephant bones show unimodal distributions with predominant peaks in the NE quadrant; while the ones from units UA3c and UB4c suggest multimodal distributions. Specifically, the UA4 sample distribution (Fig. 6b) spreads largely in the NE quadrant. Similarly, the circular distribution of the elephant sample (Fig. 6c), mainly lying in UA4, resembles the former distribution: it is skewed to the SW and concentrated in the NE quadrant. On the other hand, the UA3c sample (Fig. 6a) shows a bimodal distribution with two peaks to the E and NE, and the two samples from Area B (Fig. 6d,e) suggest a different multimodal scenario uniformly distributed.

Table 3 summarises the results of the circular uniformity tests. With regard to the UA3c sample, the Rayleigh test ( $p$  – value = 0.03) rejected the null hypothesis of circular uniformity. The mean resultant length ( $\bar{R}$  = 0.27) and the mean direction of 77°

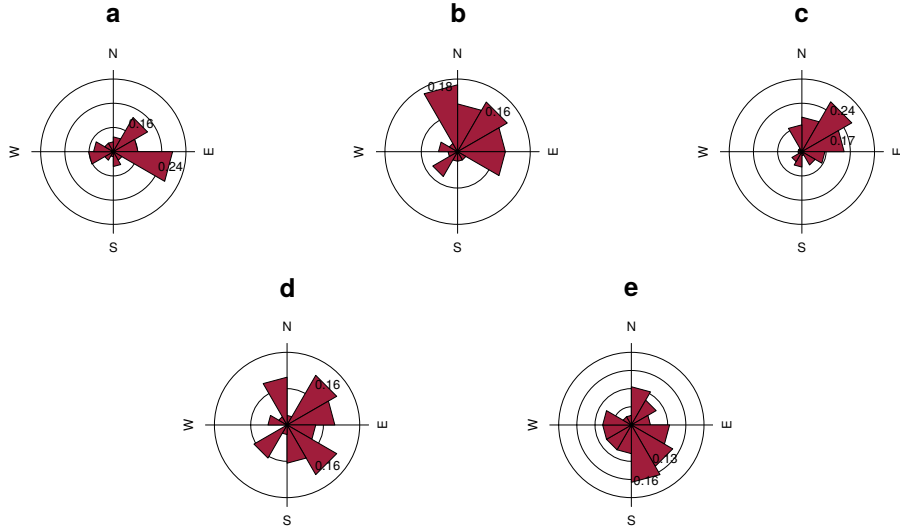


Figure 6: Rose diagrams showing the bearing patterns of samples from UA3c (a), UA4 (b), the elephant carcass (c) and UB4c (d: clock method, e: compass method).

421 are thus significant, assuming the distribution is unimodal. However, the rose diagram  
 422 (Fig. 6a) showed a bimodal distribution. The Kuiper, Watson and Rao omnibus tests,  
 423 more powerful than the Rayleigh test in detecting multimodal deviation from uniformity,  
 424 also rejected the null hypothesis of uniformity, therefore suggesting significant  
 425 anisotropy in the distribution.

426 For the UA4 sample and the subset of elephant bones, all the uniformity tests agreed  
 427 in rejecting the null hypothesis in favour of a preferentially oriented distribution. The  
 428 elephant sample, with respect to the other, showed significantly higher test results, thus  
 429 stronger anisotropy. As suggested by the rose diagrams (Fig. 6c), this sample has a  
 430 mean direction towards the NE ( $55^\circ$ ) and relatively low circular variance ( $29^\circ$ ).

431 The UB4c sub-samples had discordant test results when considering the omnibus  
 432 statistics. However, according to the Rayleigh test, the mean resultant lengths ( $\bar{R}$ )  
 433 and the mean directions were not significant for both sub-samples of measurements:  
 434  $p$ -values  $> 0.05$  failed to reject the null hypothesis of isotropy with 95% confidence  
 435 interval. This result is well confirmed by the Kuiper, Watson and Rao tests for the  
 436 sub-sample of measurements recorded using the compass. Conversely, the omnibus  
 437 tests failed to reject the hypothesis of uniformity for the other sub-sample of measure-  
 438 ments recorded with the clock method. The rose diagram (Fig. 6d) suggested for the  
 439 latter distribution strong multimodality, with uniformly spread peaks. The contrasting  
 440 results obtained for the UB4c sub-samples are most probably due to the shape of those  
 441 distributions. Indeed, the clock system, being less accurate, tends to produce a less  
 442 dense distribution, more subject to show a multimodal shape when the distribution is  
 443 actually uniform (Fig. 6a,d).

444 The Woodcock eigenvalues ratio graph (Fig. 7a) presents the shape ( $K$ ) and strength

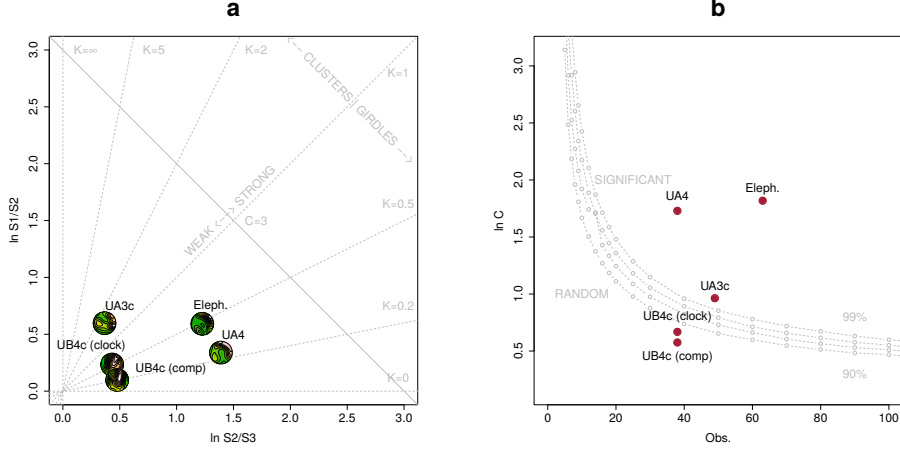


Figure 7: Woodcock's eigenvalues ratio graph (a) and plot of the Monte-Carlo critical  $S_1/S_3$  test values, for varying sample sizes and confidence levels (b), modified from [Woodcock and Naylor \(1983\)](#).

(C) of the distributions. Fig. 7b plots confidence levels of Monte-Carlo critical  $C$  values, varying for sample sizes. The two sub-samples from Area B nearly overlapped, thus suggesting reliability of the orientation measurements collected using the clock system, although of low accuracy. The two sub-samples, together with the UA3c sample, having low  $C$  values, plotted close to the origin of the ratio graph. Therefore, they indicate weak preferential orientation (UA3c) and significant randomness (UB4c). On the other hand, the UA4 and the elephant samples, with higher  $C$  values, showed a stronger and significant tendency to orient preferentially. The shape parameter  $K$  of the samples varied from  $K = 0.25$  for the UB4c sample measured with the compass, to  $K = 0.66$  for the one measured with the clock, to  $K = 0.48$  for the elephant sample. Overall, all the samples, except the UA3c one ( $K = 1.63$ ), plotted below the average shape value ( $K = 1$ ) between girdles and clusters distributions.

The Benn diagram (Fig. 8) resembles the Woodcock ratio graph (Fig. 7a). The samples from units UB4c and UA3c clearly plotted at a distance from the UA4 and the elephant samples. The UB4c samples plotted in the upper corner of the ternary graph, with the UB4c sub-sample of measurements taken with the compass exhibiting more isotropy. The UA3c sample, with an elongation index similar to the elephant sample, but higher isotropic index, plotted towards the centre. Compared to the ranges of fabrics recorded for modern natural processes (debris flow and runoff), the fabric from the UA3c and UB4c units plotted well inside the cluster of debris flows, with the UB4c (comp) sample suggesting even more random orientations. On the other hand, the sample of elephant remains, which lie mostly on UA4 and are covered by UA3c, plotted significantly close to the sample from unit UA4. They both presented the lowest isotropy index ( $IS$ ), but not high elongation index ( $EL$ ). Thus, they plotted in the average between linear and planar orientations, at the margins of the range of runoff processes. Yet they still plotted within the cluster of debris flows fabrics. Moreover, as suggested also by the uniformity tests (Tab. 3), the elephant sample showed a more

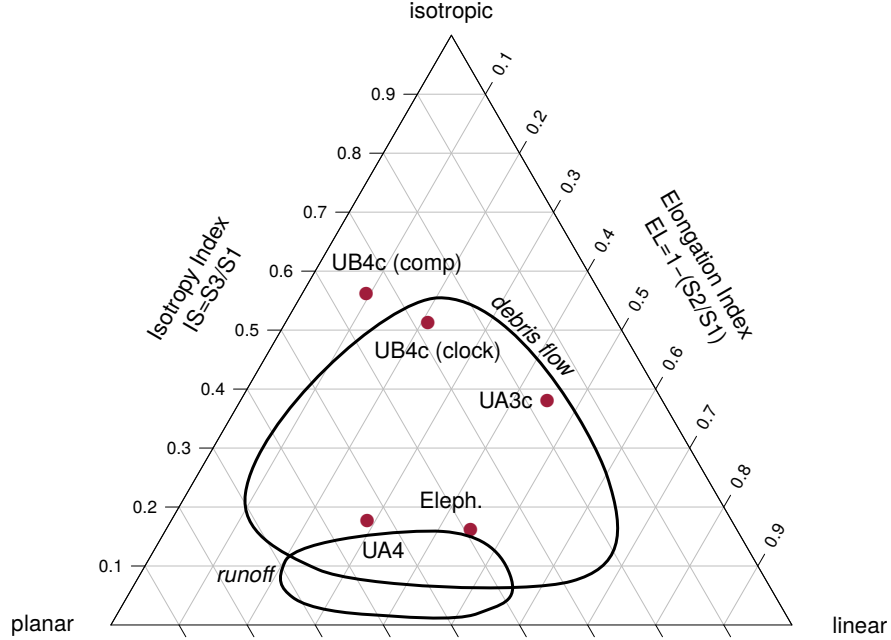


Figure 8: Benn's diagram. Fabric ranges of natural processes modified from [Lenoble and Bertran \(2004\)](#).

472 linear attitude with respect to the UA4 sample.

473 **3.2. Vertical distribution**

474 Fig. 9 compares the vertical distribution of the finds from units UA3c and UA4, by  
 475 means of empirical density functions of the minimum distances ( $d$ ) from each speci-  
 476 men to the UA3c/4 erosional contact (Fig. 5a). Three lithic artefacts (two flakes and  
 477 one tool) from the UA3c unit, not included in Fig. 9, plotted within 15 cm from the  
 478 interpolated surface. Only one flake has been found in the lower UA4, at about 17 cm  
 479 from the UA3c/4 contact, together with three chips. Despite the scarcity of debitage  
 480 products in this area, waste products (debris/chip) are relatively well represented (16%  
 481 of the UA3c sample). Their vertical dispersion approximated a normal distribution  
 482 ( $\mu = 0.24$ ,  $\sigma = 0.15$ ): the Kolmogorov-Smirnov and Shapiro tests failed to rejected  
 483 the null hypothesis of normality ( $p - value = 0.83$  and 0.075, respectively). Notably, the  
 484 distributions of the faunal remains from the same unit UA3c were all right skewed, with  
 485 means ( $\mu$ ) about 20 cm above the UA3c/4 contact. Nevertheless, the Welch two sample  
 486 t-test ( $p - value = 0.61$ ) failed to reject the null hypothesis that the lithic and faunal  
 487 sample means are equal. The total distribution of remains from unit UA3c showed a  
 488 unimodal distribution, skewed to the right, with mode in the proximity of the UA3c/4  
 489 surface. Similarly, the vertical distribution of faunal remains recovered from unit UA4  
 490 concentrate in the first 10 cm below surface. The density functions altogether clearly  
 491 confirmed one of the main observations assessed during excavation, namely that, with

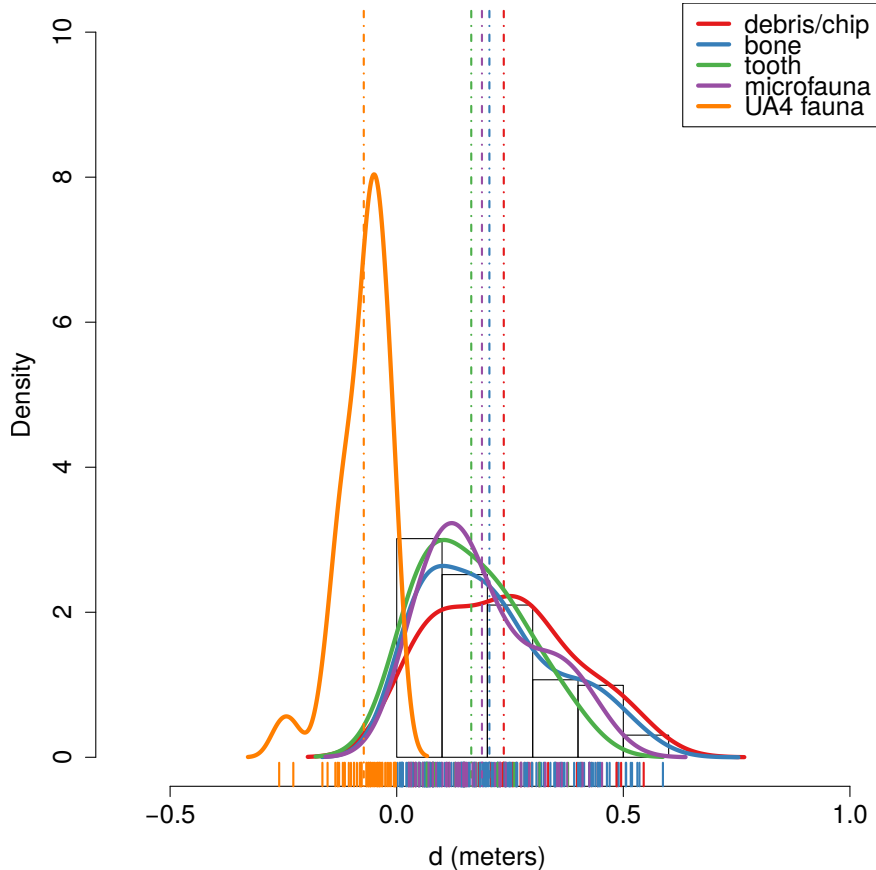


Figure 9: Empirical density functions of minimum orthogonal distances ( $d$ ) to the UA3c/4 surface. The histogram represents the total distribution of remains from UA3c; dashed lines indicate mean values.

492 the elephant remains lying at the UA3c/4 contact and covered by unit UA3c, most of  
 493 the faunal and lithic material were recovered from unit UA3c and predominantly in the  
 494 proximity of the UA3c/4 contact.

495 Fig. 10 shows the empirical density functions of the minimum distances from each  
 496 specimen from Area B to the UB4c/5a erosional contact (Fig. 5b). The combined  
 497 distribution of any type of find from the UB5a unit (Fig. 10a) skewed to the left with  
 498 a short tail (up to -0.3 m). The mode, between 5 and 10 cm below the roof of UB5a,  
 499 indicates a general concentration of material very close to the contact of this unit with  
 500 the overlying UB4c, in accordance with the mean distribution of the different classes of  
 501 remains. Although the majority of both the lithic and faunal assemblages were found  
 502 in the uppermost 15 cm of UB5a, few debris/chips and bone fragments occur lower  
 503 in the sequence, yet no more than 30 cm below the roof of this unit. Very few flakes,  
 504 three tools and no cores have been found in this unit. As a whole, the lithic assemblage

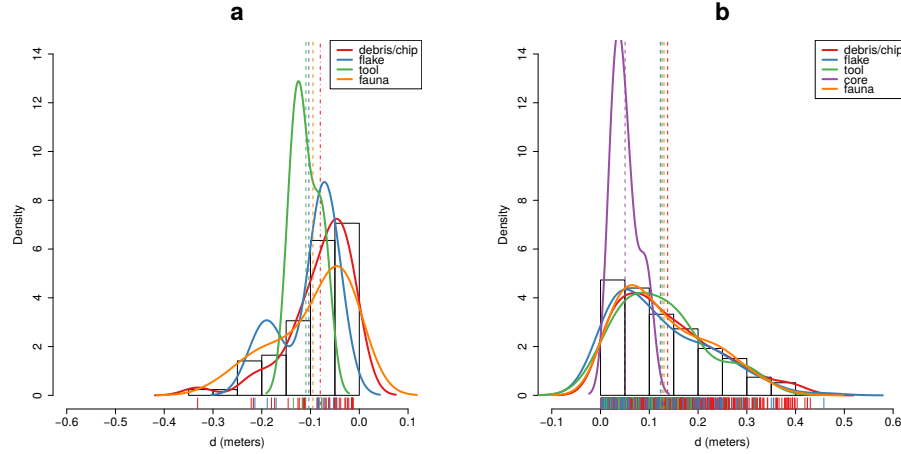


Figure 10: Empirical density functions of minimum orthogonal distances ( $d$ ) to the UB4c/5a surface. The histogram represents the total distribution of remains from UB5a (a) and UB4c (b); dashed lines indicate mean values.

505 from UB5a, mostly composed by debris/chips, is only 7% of the most conspicuous  
506 assemblage from UB4c.

507 The global distribution of unit UB4c was right skewed (up to almost 0.6 m) and  
508 centred at about 5 cm above the contact with the underlying unit UB5a (Fig. 10b).  
509 Almost 30% of the sample fell exactly at the erosional contact that separates UB4c  
510 from UB5a. The density estimations of the lithic debris/chip, flakes, tools and faunal  
511 remains significantly overlap, whereas the distribution of the six cores shows a bimodal  
512 shape with peaks at 5 and 20 cm above the contact. Moreover, the Welch Two Sample t-  
513 test of the lithic and faunal sample means failed to reject the null hypothesis ( $p$ -value =  
514 0.6295).

### 515 3.3. Point pattern analysis

516 Results of the point pattern analysis are complementary to those obtained from the  
517 analysis of the fabric and vertical distributions.

518 Regarding Area A, kernel density estimation and three-dimensional functions were  
519 applied in order to quantitatively depict the spatial distribution of the lithic assemblage  
520 in relation to the elephant skeleton.

521 Fig. 11a shows the smoothing kernel intensity estimation of the faunal assemblage  
522 from the UA3c unit. Contour lines delimit the density of the lithic sample. The partial  
523 skeleton of the *P. antiquus* is superimposed on it. A preliminary visual examination  
524 of the plot suggests a homogeneous distribution of lithics (mostly debris/chips) and  
525 fossils. Spots of higher density appear to be spread around and in association with the  
526 elephant remains.

527 The univariate pair correlation function of the joined lithic assemblage from the  
528 UA3c and UA4 units (Fig. 11b) suggests aggregation of finds. The estimated  $\hat{g}_3(r)$   
529 function (black solid line) wanders above the benchmark value (red dotted line) until

values of  $r = 0.8$ . However, for distances between 35 and 65 cm, it lies above the grey envelope of significance for the null hypothesis of CSR, indicating that at those distances artefacts occur significantly closer than expected in the case of random processes. For values of  $r > 0.8$ , the function stabilises at values close to 0, suggesting a Poisson distribution. The plot illustrates the random distribution of finds between patches of clusters that we observe in Fig. 11a.

The histogram in Fig. 11c shows the density of the distances calculated from each artefact to the nearest-neighbour elephant remain. A right skewed distribution, with a prevalent peak at 10 cm and mean ( $\mu$ ) 30 cm is an indication of the relatively strong aggregation of lithics around the mass of the elephant skeleton.

As for Area B, the analysis focused on the spatial distribution and cross-correlation of the assemblages from UB4c and UB5a (Fig. 12).

Figs. 12a,b respectively show kernel density estimations of the combined lithic and faunal assemblages from both the units analysed. Despite the samples size difference, a first visual examination suggests the presence of interesting spatial structures.

Regarding the UB4c unit (Fig. 12a), the high density of material concentrated around the western square 934/600 suggests that the pattern could have been the result of an inhomogeneous, non-uniform depositional process. Visual comparison of the density plot with the elevation model of the erosional contact between the UB4c and UB5a units (Fig. 5b) suggests positive correlation between lower elevations (topographic depressions) and higher density of remains. Fig. 12c shows the results of the  $\rho$ -function, which estimates the intensity of the UB4c sample assemblage as a function of the covariate underlying topography created by the erosional event. Within the range of elevation between 350.2 and 350.4 m, the occurrence of finds is higher and the intensity decreases with the rise of elevation, i.e., finds are more likely to be found at lower elevations than would be expected if the intensity was constant.

Spatial Kolmogorov-Smirnov (KS) and Berman's  $Z_2$  (Berman, 1986) statistics were used in order to test the dependence of the UB4c pattern on the covariate erosional surface. Both KS ( $D = 0.11952$ ,  $p - value = 7.772e - 16$ ) and  $Z_2$  ( $Z_2 = -7.8447$ ,  $p - value = 4.34e - 15$ ) significantly rejected the null hypothesis of CSR. Although the tests suggested evidence that the intensity depends on the covariate, the effect of the covariate is weak and it seems to have no discriminatory power. The ROC curve and AUC statistics (0.56), which measure the strength of the covariate effect, suggest that the underlying UB4c/5a topography does not completely explain the localised high density of occurrence in the UB4c.

Relative spatial segregation seems to occur between the assemblages from UB4c (Fig. 12a) and UB5a (Fig. 12b), with high density of the former distribution corresponding to low density of the latter. The former analysis of the vertical distribution showed that the two assemblages occur very close to their stratigraphic contact. In order to further investigate the spatial interaction between the two depositional events, we applied multitype pair correlation ( $g_{ij}(r)$ ) and nearest-neighbour ( $G_{ij}(r)$ ) functions.

Fig. 12d shows the estimated values of the multivariate  $\hat{g}_{ij}(r)$  function against the envelope of the null hypothesis, obtained by randomly shifting the position of remains from the two distributions in 199 Monte Carlo simulations. For fixed values of  $r$  less than 30 cm the observed function lies below the benchmark value of independence, thus indicating segregation; but it wanders at the lower edge of the grey envelope. For fixed

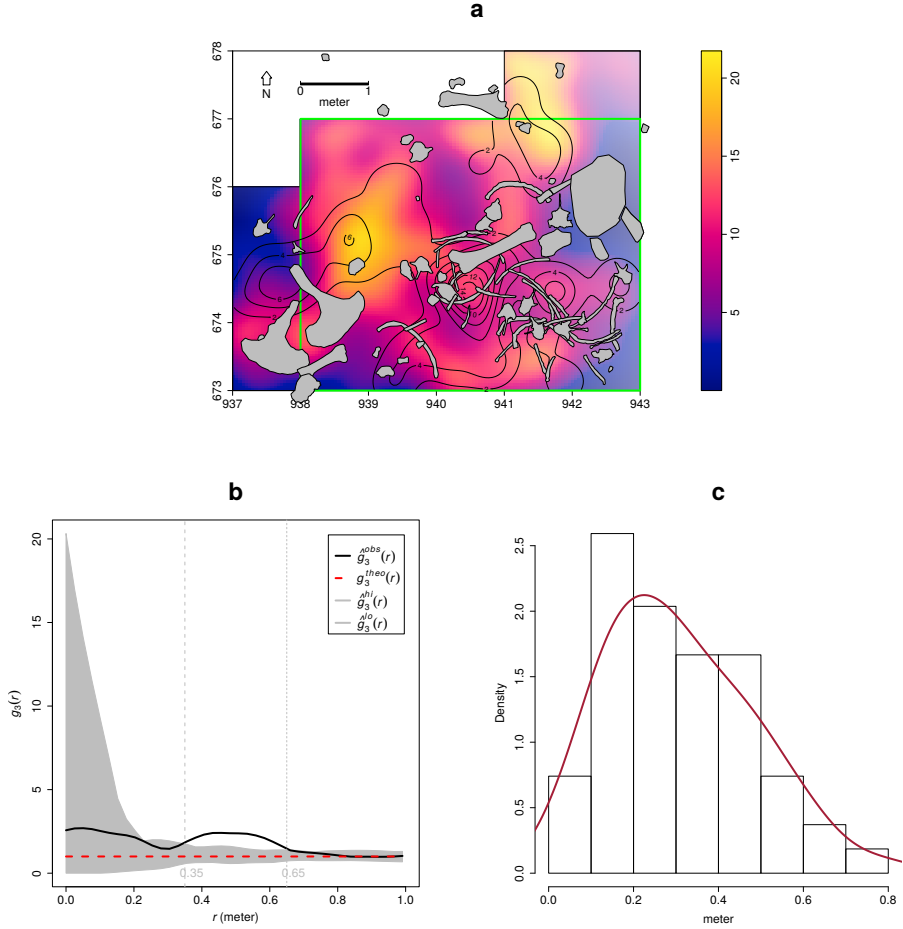


Figure 11: Kernel smoothed intensity function of the faunal assemblages from UA3c. Isolines mark the density of the lithic artefacts from UA3c (a). Pair correlation function ( $g_3(r)$ ) of a three-dimensional pattern of lithic artefacts from UA3c and UA4. Grey envelope of 999 Monte Carlo simulations under the CSR null hypothesis (b). Three-dimensional distance from each lithic artefact from UA3c and UA4 to the nearest neighbour elephant remain (c).

576 distances of  $r > 0.3$  m the observed and theoretical lines significantly overlap. Overall,  
577 the function suggests independence of the two point processes (UB4c and UB5a) at  
578 multiple scales.

579 However, the estimated  $\hat{G}_{ij}(r)$  function (Fig. 12c), running well below the signifi-  
580 cance grey envelope for fixed values of  $r > 0.3$  m, confirms that the nearest-neighbour  
581 distances between remains from UB4c and UB5a are significantly longer than expected  
582 in the case of independent processes. Interestingly, at values of  $r < 0.2$  m the observed  
583 function failed to reject the null hypothesis of Complete Spatial Randomness and In-  
584 dependence (CSR).

#### 585 4. Discussion

586 Recent excavations at the Middle Pleistocene site of Marathousa 1 have unearthed  
587 in one of the two investigated areas (Area A) a partial skeleton of a single individual  
588 of *Palaeoloxodon antiquus*, whose bones are in close anatomical association, and spa-  
589 tially and stratigraphically associated with lithic artefacts and other faunal remains. In  
590 Area B, 60 m to the South of Area A, we collected a much higher number of lithic  
591 artefacts (Tourloukis et al., this issue), spatially and stratigraphically associated with  
592 other faunal remains, including isolated elephant bones, cervids and carnivores among  
593 others (Konidaris et al., this issue). The two areas are stratigraphically correlated, the  
594 main fossiliferous layers (UA3c and UB4c) representing a massive depositional pro-  
595 cess, such as a hyperconcentrated flow that dumped material in a lake margin context  
596 (Karkanas et al., this issue). To date, evidence of butchering (cut-marks) has been iden-  
597 tified on two bones of the elephant skeleton from Area A, as well on elephant and other  
598 mammal bones from Area B (Konidaris et al., this issue).

599 However, due to the secondary depositional nature of the main fossiliferous hori-  
600 zon, it is of primary importance to evaluate the degree and reliability of the spatial  
601 association of the lithic artefacts with the faunal remains, and especially with the ele-  
602 phant skeleton. In order to tackle our main objective, we applied a comprehensive  
603 set of spatial statistics to the distributions of the archaeological and zooarchaeologi-  
604 cal/palaeontological remains from relevant stratigraphic units of the two areas of in-  
605 vestigation. Preliminary results of our analyses are here discussed for both areas.

##### 606 4.1. Fabric analysis

607 The analysis of the orientation (plunge and bearing) of subsets of remains, mostly  
608 bone, wood fragments and lithic artefacts, showed different patterns for the two main  
609 find-bearing units.

610 In Area B, two sub-samples from the same stratigraphic unit were analysed, in order  
611 to asses the reliability of the orientation data measured with the clock system. Due to  
612 the different shapes of the distributions (Figs. 6d,e), test statistics reported contrasting  
613 results (Tab. 3). Indeed, the clock system, recording non-continuous circular data,  
614 tends to produce a distribution more subject to show a multimodal shape when it is  
615 actually uniform. However, the two sub-samples nearly overlapped when plotted in  
616 the three-dimensional Woodcock (Fig. 7) and Benn (Fig. 8) diagrams, thus suggesting  
617 some degree of reliability of the clock method. Nevertheless, despite minor differences  
618 between the two samples, caution should be paid in analysing grouped circular data.

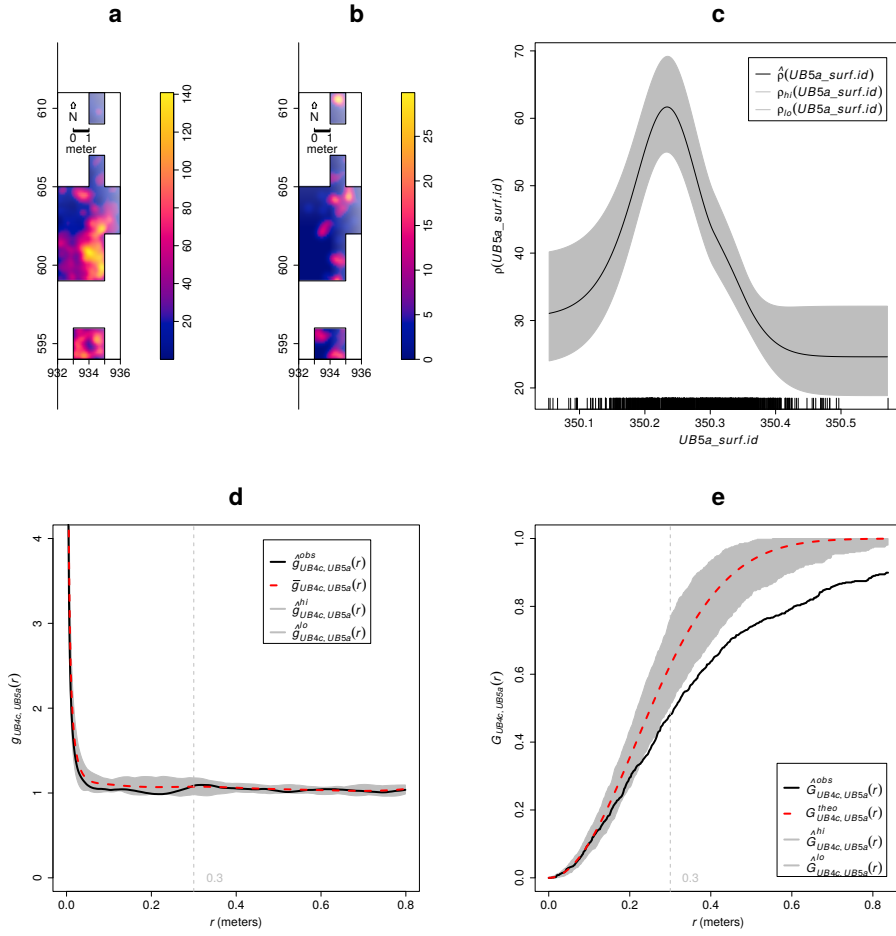


Figure 12: Kernel smoothed intensity function of the lithic and faunal assemblages from UB4c (a) and UB5a (b). Smoothing estimate of the intensity of remains from UB4c, as a function of the erosional surface UB4c/5a. Grey shading is point-wise 95% confidence bands (c). Cross-pattern pair correlation function ( $g_{ij}(r)$ ) between the UB4c and UB5a distributions. Grey envelope of 199 Monte Carlo simulations under the independence of components null hypothesis (d). Multitype nearest-neighbour function ( $G_{ij}(r)$ ) between the UB4c and UB5a distributions (e).

619 The test results (Tab. 3) for the UA4 sample and the sample of elephant remains  
620 - which lie on unit UA4 and are covered by UA3c - indicated significant preferential  
621 orientations towards the NE (Figs. 6b,c). As shown by the Woodcock's (Fig. 7) and the  
622 Benn's diagrams (Fig. 8), these samples plotted together at a distance from the others.  
623 Such convergence suggests that the elephant carcass, the other faunal remains and the  
624 organic material, deposited on unit UA4, were subject to the same processes.

625 Far from the isotropic corner in the Benn's diagram these two samples from Area  
626 A plotted approximately in between the linear and planar extremes, with the elephant  
627 sample showing a more linear fabric. When the results published by Bertran et al.  
628 (1997) and Lenoble and Bertran (2004) from observations of fabrics in modern sub-  
629 aereal slope deposits were used as a reference, the two samples aggregated at the ex-  
630 treme margins of runoff processes. Yet, they plotted well within the cluster of debris  
631 flows and relatively distant from the linear corner.

632 Although Bertran et al. (1997) studied runoff deposits from different environments  
633 (channel-lag gravels in rills, small gullies, and inter-rill surfaces on alpine slopes; and  
634 faintly laminated gravel lenses on an inactive, small colluvial fan), this result is consis-  
635 tent with the exposure of unit UA4 to overland water-laden processes that occurred be-  
636 fore the flood event UA3c/UB4c. Notably, the erosive nature of low-energy processes  
637 triggered by rain-water has been observed on lacustrine floodplains, and is associated  
638 with anisotropic patterns in autochthonous assemblages (Cobo-Sánchez et al., 2014;  
639 Domínguez-Rodrigo et al., 2014c; García-Moreno et al., 2016).

640 Pockets of thinly bedded organic-rich silty sands have been found mixed in UA4.  
641 These sands in Area A resemble the UB5b/c sandy deposit in Area B, which is associ-  
642 ated with relatively high energy fluvial flows entering the lake margins (Karkanas et al.,  
643 this issue). Eventually, such relatively high energy flood (UB5b/c) would have had the  
644 power to significantly reorient elements of the elephant carcass and slightly displace  
645 them. However, the elephant skeleton clearly lies on top of unit UA4 and is covered by  
646 UA3c (see Fig.4).

647 Moreover, unlike bones with a tubular shape (i.e., long bones), ribs and vertebrae  
648 are prone to orient preferentially under high energy processes, less likely under low  
649 energy processes (Domínguez-Rodrigo and García-Pérez, 2013; Domínguez-Rodrigo  
650 et al., 2014c). Interestingly, whereas some of the ribs share the same preferential orien-  
651 tation with the long bones, others are oriented NW/SE. However, a NW/SE orientation  
652 could be consistent with a prevalent NE direction of the flow (and vice-versa), since  
653 long bones could roll orthogonally to the flow direction (Voorhies, 1969). On the other  
654 hand, a higher energy flood would lead to an under-representation of carpals, tarsals,  
655 metapodials, phalanges, ribs and vertebrae, which are more prone - when disarticulated  
656 - to be easily transported by water induced processes (Voorhies, 1969). Yet, several of  
657 these bones are present and in close spatial association with the elephant cranium and  
658 other skeletal elements. The presence of many of the skeletal elements with different  
659 transportation properties suggests that the elephant carcass was not subjected to high  
660 energy processes before the flood event UA3c/UB4c.

661 The fabrics of the UA3c and UB4c samples, with higher isotropic index (*IS*), plot-  
662 ted at a significant distance from the elephant sample, yet within the cluster of debris  
663 flows (Fig. 8). Indeed, random distribution and orientation of clasts is expected for de-  
664 bris flows, except at flow margins, where preferential orientation and clusters of clasts

have been observed (Pierson, 2005). However, hyperconcentrated flows, such as the UA3c/UB4c flood event, which fall in between the spectrum of water and debris flows, may develop parallel or normal orientation to the flow direction (Lindsay, 1968; Benvenuti and Martini, 2002). Notably, with respect to the UB4c sample, the UA3c sample exhibits a higher elongation index ( $ES$ ), similar to that of the elephant sample (Fig. 8). Rose diagrams (Fig. 6) and uniformity tests (Tab. 3) also suggest similar fabrics of the samples from Area A.

Thus, we can assume that an overland flow, namely UA3c/UB4c, is likely to have slightly reworked and preferentially oriented to the NE the exposed elements of the already dismembered (and probably already marginally displaced) elephant carcass, which mostly preserves close anatomical associations, but not anatomical connections.

Although little is currently known about the spatial extension of the UA3c/UB4c flow event, the different orientation patterns between the two areas could probably be explained with lateral variability. Indeed, the same event could exhibit different behaviours at different temporal and spatial points, giving rise to different distribution patterns.

As suggested by Lenoble and Bertran (2004), fabric analysis is not sufficient to unequivocally discriminate processes and should therefore be integrated with the analysis of other diagnostic features.

#### 4.2. Vertical distribution

As for the vertical distribution, we assumed that mass processes, such as hyperconcentrated flows, would predominantly distribute poor to very poor sorted clasts homogeneously throughout the sequence (Pierson, 2005). Diagnostic inverse grading, or a continuously aggrading bed can be observed in the resultant deposits (Benvenuti and Martini, 2002). A concentration of unsorted elements in the proximity of the erosional surface, as well as the absence of any grading, would in turn suggest an autochthonous assemblage.

The lithic assemblage from Area A - the combined units UA3c and UA4 ( $n = 54$ ), composed by a few debitage products and a relatively high number of debris/chips and retouch waste products (Tab. 2) - plotted predominantly in the proximity of the erosional surface created by the UA3c/UB4c event (Fig. 5a). The faunal remains from unit UA3c resemble the distribution of the archaeological assemblage; whereas the ones from the underlying unit UA4 plotted within 10 cm below the erosional contact. Overall, the material recovered from unit UA3c did not show any grading and mainly plotted at the bottom of the unit (Fig. 9). Thus, its vertical distribution is consistent with the hypothesis of an autochthonous assemblage.

In Area B, two samples from units UB4c ( $n = 1243$ ) and UB5a ( $n = 101$ ) respectively, were analysed (Tab. 2) for quantifying the minimum orthogonal distance of each item to the modelled erosional surface (Fig. 5b).

The vertical distribution of lithic artefacts and fossils from unit UB4c showed a predominant peak right at the contact with the erosional surface. Almost 30% of this rich sample plotted at a distance between 0 and 5 cm from the erosional contact; whereas the rest gently skewed to the upper part of the unit, up to about 50 cm. The same distribution was observed for all classes of remains, suggesting no size sorting and an origin very close to the erosional surface (Fig. 10b).

710 The density distribution of the sample from the underlying UB5a unit (Fig. 10a)  
711 globally indicates a more constrained vertical displacement of remains (within 30 cm  
712 below the erosional surface). Whereas lithic artefacts and fossils mostly plot right at  
713 the contact and just below it, a few debris/chips and faunal remains were found lower  
714 in the sequence. No size sorting was observed, but, notably, lithic cores are absent and  
715 the debris/chip distribution is wider than the distribution of the few flakes and tools.

716 Field observations of cracks in the clayey UB5a unit testify to shrinking and swelling  
717 during wet and dry cycles (Karkanas et al., this issue), which suggests that vertical dis-  
718 placement of some small lithics and fossil fragments at lower depths with respect to  
719 the UB5a/4c contact probably resulted from clay desiccation.

720 Likewise, Lenoble and Bertran (2004) documented up to 30 cm vertical dispersion  
721 and frequent vertical plunge of artefacts from the marshy silty clay of the Croix-de-  
722 Canard site, sector 3. Furthermore, a recent experimental study of animal trampling  
723 in water saturated substrates reported negative correlation with artefact size, signifi-  
724 cant inclination and greater vertical displacement than any former work: a maximum  
725 between 16 and 21 cm, with a mean of about 6 cm (Eren et al., 2010).

726 The fact that the majority of the remains from units UB4c and UB5a plotted at, or  
727 very close to the contact between these two layers, the relatively high percentage of  
728 lithics in both units, as well as the absence of grading, suggest autochthonous assem-  
729 blages, deposited in UB5a and subsequently eroded *in situ* by the UA3c/UB4c flood  
730 event.

#### 731 4.3. Point pattern analysis

732 The autochthonous hypothesis was further explored by means of point pattern  
733 analysis. According to this model, in both areas the lithic and faunal assemblages  
734 were primarily deposited *in situ* and were subsequently eroded and re-deposited (*sensu*  
735 Fernández-López, 1991) by the hyperconcentrated flow UA3c/UB4c. We assumed  
736 that a completely random spatial distribution of the lithic artefacts and faunal remains  
737 would suggest an allochthonous origin and subsequent re-elaboration (*sensu* Fernández-  
738 López, 1991), with transport to the site by the action of a random massive process.  
739 Nevertheless, clustering of artefacts is not necessarily evidence of human presence.  
740 Aggregation or segregation patterns could be produced by a range of biotic and/or nat-  
741 ural processes. Human activities, topography and physical obstructions alike could  
742 trigger spatial aggregation.

743 The three-dimensional distribution of lithic artefacts from unit UA3c shows signif-  
744 icant clustering for values of  $r$  between 35 and 65 cm. Lithic artefacts occur relatively  
745 close to the skeletal elements of the elephant, at a distance between 20 and 50 cm at  
746 most (Fig. 11). The richest cluster of about 20 lithic artefacts is located to the SW of  
747 the cranium, close to the right femur and the scatter of ribs and vertebrae.

748 Considering the prevalent NE orientation of the elephant bones and the other fau-  
749 nal remains from UA4 and UA3c, it is not unlikely that a SW/NE oriented flood could  
750 have been responsible for the observed accumulation to the SW of the elephant cra-  
751 nium, which would have represented an important obstruction to the flow. A similar  
752 case of clustering of small remains, apparently dammed by a long elephant tusk, has  
753 also been observed at Castel di Guido (Italy) (Boschian and Saccà, 2010). Secondary

754 deposition by low-energy flows and clustering of artefacts and bones blocked by an  
755 aurochs carcass have been as well documented at the site of 'Ein Qashishadd (Israel)  
756 ([Hovers et al., 2014](#)).

757 However, the pair correlation function (Fig. 9b) suggests significant clustering of  
758 lithic artefacts at relatively small scale: a pattern less likely to be produced by a large  
759 scale massive process such as a hyperconcentrated flow. Moreover, clusters of lithic  
760 artefacts occur as well in areas with lower densities of elephant bones.

761 Small scale clustering; proximity to the elephant remains and the erosional sur-  
762 face; absence of spatial size sorting and, on the contrary, the presence of a relatively  
763 high number of lithic debris/chips associated with some flakes, tools and a rich fau-  
764 nal assemblage; close anatomical spatial association of the elephant skeletal elements,  
765 slightly displaced and preferentially oriented: altogether these lines of evidence support  
766 the hypothesis of an autochthonous deposition, subject to localised minor reworking.

767 A similar pattern can be observed in Area B, where an initial set of spatial statistics  
768 confirmed that the inhomogeneous density of remains from unit UB4c (Fig. 12a) is  
769 not completely explained by the covariate effect of the underlying complex topography  
770 created by the erosional event UA3c/UB4c (Fig. 5b).

771 Thus, we explored the relative spatial interaction between the UB4c and the un-  
772 derlying UB5a samples. We assumed that complete spatial randomness of the two  
773 independent depositional processes would occur in case of an allochthonous origin and  
774 transportation of the UB4c assemblage. The hypothesis of an autochthonous original  
775 deposition of the faunal and lithic assemblages on the UB5a unit, subsequently eroded  
776 *in situ* by a relatively high energy flood (UB4c), was tested by cross-pattern spatial  
777 correlation functions (Figs. 12d,e). Whereas the two samples are vertically adjacent to  
778 the erosional surface (Fig. 10), on the horizontal plane they are both more segregated  
779 than expected for a random distribution.

780 Conversely, the extraordinary preservation and number of mint to sharp, unsorted  
781 lithic artefacts from the UB4c unit; their density, positively correlated to the topog-  
782 raphy, and significantly segregated from the underlying distribution of remains; the  
783 vertical proximity of both assemblages from UB4c and UB5a to the erosional surface;  
784 as well as the random orientation pattern of the former, suggest that significant dis-  
785 placement of materials due to the erosional event can be excluded.

786 The faunal and lithic assemblages from unit UB4c therefore most likely derived  
787 from the local erosion of exposed mudflat areas (unit UB5a) and have been slightly  
788 redistributed by the same flood event that capped the elephant in Area A.

789 Further evidence that the recovered assemblage has not undergone substantial re-  
790 working and has retained its original characteristics would come from the refitting anal-  
791 ysis, currently in progress. To date, 4 bone refits have been found in Area B: three from  
792 unit UB4c, respectively at 4.77, 0.05 and 0.01 m distance; and one between two mam-  
793 mal bone fragments from units UB4c and UB5a, at a very short distance (0.09 m).  
794 Interestingly, one of the elements of the most distant refit (a *Dama* sp. mandibular  
795 fragment) shows traces of carnivore gnawing ([Konidaris et al., this issue](#)).

796 In conclusion, multiple lines of evidence reject an allochthonous hypothesis of de-  
797 position in favour of an autochthonous model. The erosional event UA3c/UB4c repre-  
798 sents an *en masse* depositional process, i.e. a hyperconcentrated flow, in the continuum  
799 between water and debris flow, which would have locally reworked at a small scale

800 the already exposed or slightly buried and spatially associated lithic and faunal assem-  
801 blages.

802 Although the UA3c/UB4c process represents a snapshot of a relatively short time-  
803 frame, high resolution inferences about the use of space by human groups, in terms  
804 of knapping episodes and butchering activities, are unreliable in light of the current  
805 information.

806 The spatial pattern observed at the site is indeed the result of the last episode in a  
807 palimpsest of spatial processes. Whereas the erosional event represented by the hyper-  
808 concentrated flow UA3c/UB4c caps the fossiliferous horizon and preserves the record,  
809 little is known about the underlying, eroded 'occupational' surface.

810 However, whereas hunting or scavenging in the Lower Palaeolithic is still an un-  
811 solved matter of debate, considering the rate of bone fragmentation, the density of lithic  
812 debris/chips, the number of processed bones and their spatial density and association, it  
813 is likely that the assemblage represents a complex palimpsest of locally repeated events  
814 of hunting/scavenging and exploitation of lake shore resources.

815 More data from high resolution excavations in the coming years will allow us to  
816 refine the coarse-grained spatio-temporal resolution of our inferences about past human  
817 behaviour at Marathousa 1.

## 818 5. Conclusions

819 At the Middle Pleistocene open-air site of Marathousa 1, a partial skeleton of a  
820 single individual of *Palaeoloxodon antiquus* was recovered in stratigraphic association  
821 with a rich and consistent lithic assemblage and other vertebrate remains. Cut-marks  
822 and percussion marks have been identified on the elephant and other mammal bones ex-  
823 cavated at the site. The main find-bearing horizon represents a secondary depositional  
824 process in a lake margin context.

825 Understanding the site formation processes is of primary importance in order to  
826 reliably infer hominin exploitation of the elephant carcass and other animals. To meet  
827 this aim, we applied a comprehensive set of multivariate and multiscale spatial analyses  
828 in a taphonomic framework.

829 Results from the fabric, vertical distribution and point pattern analyses are consis-  
830 tent with a relatively high-energy erosional process slightly reworking at a small scale  
831 an exposed (or slightly buried) and consistent scatter of lithic artefacts and faunal re-  
832 mains. These results are in agreement with preliminary taphonomic observations of the  
833 lithic artefacts ([Tourloukis et al., this issue](#)) and the faunal remains ([Konidaris et al.,](#)  
834 [this issue](#)), which also indicate minor weathering and transportation. Our analyses  
835 show that multiple lines of evidence support an autochthonous origin of the lithic and  
836 faunal assemblages, subject to minor post-depositional reworking.

## 837 Acknowledgements

838 This research is supported by the European Research Council (ERC StG PaGE  
839 283503) awarded to K. Harvati. We are grateful to the Municipality of Megalopolis,  
840 the authorities of the Region of Peloponnese, and the Greek Public Power corpora-  
841 tion (ΔΕΗ) for their support. We also thank Julian Bega and all the participants in the

842 PaGE survey and excavation campaigns in Megalopolis for their indispensable coop-  
843 eration. We are grateful to the editors and two anonymous reviewers for their critical  
844 discussions and many constructive comments that helped to improve this manuscript.

845 **References**

- 846 Anderson, K. L., Burke, A., 2008. Refining the definition of cultural levels at Karabi  
847 Tamchin: a quantitative approach to vertical intra-site spatial analysis. *Journal of*  
848 *Archaeological Science* 35 (8), 2274–2285.
- 849 Aramendi, J., Uribelarrea, D., Arriaza, M. C., Arráiz, H., Barboni, D., Yravedra, J.,  
850 Ortega, M. C., Gidna, A., Mabulla, A., Baquedano, E., Domínguez-Rodrigo, M.,  
851 2017. The paleoecology and taphonomy of AMK (Bed I, Olduvai Gorge) and its  
852 contributions to the understanding of the “Zinj” paleolandscape. *Palaeogeography,*  
853 *Palaeoclimatology, Palaeoecology* (in press).
- 854 Baddeley, A., Chang, Y.-M., Song, Y., Turner, R., 2012. Nonparametric estimation of  
855 the dependence of a point process on spatial covariates. *Statistics and Its Interface*  
856 5 (2), 221–236.
- 857 Bailey, G., 2007. Time perspectives, palimpsests and the archaeology of time. *Journal*  
858 *of Anthropological Archaeology* 26 (2), 198–223.
- 859 Bar-Yosef, O., Tchernov, E., 1972. On the palaeo-ecological history of the site of Ubei-  
860 diya. Vol. 35. Israel Academy of Sciences and Humanities, Jerusalem.
- 861 Bargalló, A., Gabucio, M. J., Rivals, F., 2016. Puzzling out a palimpsest: Testing an  
862 interdisciplinary study in level O of Abric Romaní. *Quaternary International* 417,  
863 51–65.
- 864 Benito-Calvo, A., de la Torre, I., 2011. Analysis of orientation patterns in Olduvai  
865 Bed I assemblages using GIS techniques: Implications for site formation processes.  
866 *Journal of Human Evolution* 61 (1), 50–60.
- 867 Benito-Calvo, A., Martínez-Moreno, J., Mora, R., Roy, M., Roda, X., 2011. Trampling  
868 experiments at Cova Gran de Santa Linya, Pre-Pyrenees, Spain: their relevance for  
869 archaeological fabrics of the Upper–Middle Paleolithic assemblages. *Journal of Ar-  
870 chaeological Science* 38 (12), 3652–3661.
- 871 Benito-Calvo, A., Martínez-Moreno, J., Pardo, J. F. J., de la Torre, I., Torcal, R. M.,  
872 2009. Sedimentological and archaeological fabrics in Palaeolithic levels of the  
873 South-Eastern Pyrenees: Cova Gran and Roca del Bous Sites (Lleida, Spain). *Jour-*  
874 *nal of Archaeological Science* 36 (11), 2566–2577.
- 875 Benn, D., 1994. Fabric shape and the interpretation of sedimentary fabric data. *Journal*  
876 *of Sedimentary Research* 64 (4a), 910–915.

- 877 Benvenuti, M., Martini, I. P., 2002. Analysis of terrestrial hyperconcentrated flows and  
878 their deposit. In: Martini, I. P., Baker, V. R., Garzón, G. (Eds.), Flood and Megaflood  
879 Processes and Deposits. Vol. 32 of Special Publication of the International Associa-  
880 tion of Sedimentologists. Blackwell Publishing Ltd., pp. 167–193.
- 881 Berman, M., 1986. Testing for spatial association between a point process and another  
882 stochastic process. *Applied Statistics* 35, 54–62.
- 883 Bernatchez, J. A., 2010. Taphonomic implications of orientation of plotted finds from  
884 Pinnacle Point 13B (Mossel Bay, Western Cape Province, South Africa). *Journal of*  
885 *Human Evolution* 59 (3–4), 274–288.
- 886 Bertran, P., Hetù, B., Texier, J.-P., Steijn, H. V., 1997. Fabric characteristics of subaerial  
887 slope deposits. *Sedimentology* 44 (1), 1–16.
- 888 Bertran, P., Texier, J.-P., 1995. Fabric Analysis: Application to Paleolithic Sites. *Jour-*  
889 *nal of Archaeological Science* 22 (4), 521–535.
- 890 Bevan, A., Crema, E., Li, X., Palmisano, A., 2013. Intensities, Interactions, and Un-  
891 certainties: Some New Approaches to Archaeological Distributions. In: Bevan, A.,  
892 Lake, M. (Eds.), Computational Approaches to Archaeological Spaces. Left Coast  
893 Press, Walnut Creek, pp. 27–52.
- 894 Binford, L. R., 1981. Behavioral Archaeology and the "Pompeii Premise". *Journal of*  
895 *Anthropological Research* 37 (3), 195–208.
- 896 Boschian, G., Saccà, D., 2010. Ambiguities in human and elephant interactions? Sto-  
897 ries of bones, sand and water from Castel di Guido (Italy). *Quaternary International*  
898 214 (1–2), 3–16.
- 899 Brantingham, P. J., Surovell, T. A., Waguespack, N. M., 2007. Modeling post-  
900 depositional mixing of archaeological deposits. *Journal of Anthropological Archae-  
901 ology* 26 (4), 517–540.
- 902 Carrer, F., 2015. Interpreting Intra-site Spatial Patterns in Seasonal Contexts: an Eth-  
903 noarchaeological Case Study from the Western Alps. *Journal of Archaeological*  
904 *Method and Theory*, 1–25.
- 905 Cobo-Sánchez, L., Aramendi, J., Domínguez-Rodrigo, M., 2014. Orientation patterns  
906 of wildebeest bones on the lake Masek floodplain (Serengeti, Tanzania) and their  
907 relevance to interpret anisotropy in the Olduvai lacustrine floodplain. *Quaternary*  
908 *International* 322–323 (Supplement C), 277–284.
- 909 de la Torre, I., Benito-Calvo, A., 2013. Application of GIS methods to retrieve ori-  
910 entation patterns from imagery; a case study from Beds I and II, Olduvai Gorge  
911 (Tanzania). *Journal of Archaeological Science* 40 (5), 2446–2457.
- 912 Dibble, H. L., Chase, P. G., McPherron, S. P., Tuffreau, A., Oct. 1997. Testing the  
913 reality of a "living floor" with archaeological data. *American Antiquity* 62 (4), 629–  
914 651.

- 915 Diggle, P., 1985. A kernel method for smoothing point process data. *Applied Statistics*  
916 (Journal of the Royal Statistical Society, Series C) 34, 138–147.
- 917 Domínguez-Rodrigo, M., Bunn, H., Mabulla, A., Baquedano, E., Uribelarrea, D.,  
918 Pérez-González, A., Gidna, A., Yravedra, J., Diez-Martín, F., Egeland, C., Barba,  
919 R., Arriaza, M., Organista, E., Ansón, M., 2014a. On meat eating and human evolution:  
920 A taphonomic analysis of BK4b (Upper Bed II, Olduvai Gorge, Tanzania), and  
921 its bearing on hominin megafaunal consumption. *Quaternary International* 322–323,  
922 129–152.
- 923 Domínguez-Rodrigo, M., Bunn, H., Pickering, T., Mabulla, A., Musiba, C., Baquedano,  
924 E., Ashley, G., Diez-Martín, F., Santonja, M., Uribelarrea, D., Barba, R.,  
925 Yravedra, J., Barboni, D., Arriaza, C., Gidna, A., 2012. Autochthony and orientation  
926 patterns in Olduvai Bed I: a re-examination of the status of post-depositional biasing  
927 of archaeological assemblages from FLK North (FLKN). *Journal of Archaeological  
928 Science* 39 (7), 2116–2127.
- 929 Domínguez-Rodrigo, M., Cobo-Sánchez, L., Yravedra, J., Uribelarrea, D., Arriaza, C.,  
930 Organista, E., Baquedano, E., 2017. Fluvial spatial taphonomy: a new method for the  
931 study of post-depositional processes. *Archaeological and Anthropological Sciences*.
- 932 Domínguez-Rodrigo, M., Diez-Martín, F., Yravedra, J., Barba, R., Mabulla, A., Baquedano,  
933 E., Uribelarrea, D., Sánchez, P., Eren, M. I., 2014b. Study of the SHK Main  
934 Site faunal assemblage, Olduvai Gorge, Tanzania: Implications for Bed II taphonomy,  
935 paleoecology, and hominin utilization of megafauna. *Quaternary International*  
936 322–323, 153–166.
- 937 Domínguez-Rodrigo, M., García-Pérez, A., 07 2013. Testing the Accuracy of Different  
938 A-Axis Types for Measuring the Orientation of Bones in the Archaeological and  
939 Paleontological Record. *PLoS ONE* 8 (7), e68955.
- 940 Domínguez-Rodrigo, M., Uribelarrea, D., Santonja, M., Bunn, H., García-Pérez, A.,  
941 Pérez-González, A., Panera, J., Rubio-Jara, S., Mabulla, A., Baquedano, E., Yrave-  
942 dra, J., Diez-Martín, F., 2014c. Autochthonous anisotropy of archaeological ma-  
943 terials by the action of water: experimental and archaeological reassessment of the  
944 orientation patterns at the Olduvai sites . *Journal of Archaeological Science* 41 (Sup-  
945 plement C), 44–68.
- 946 Eberth, D. A., Rogers, R. R., Fiorillo, A. R., 2007. A practical approach to the study of  
947 bonebeds. In: Rogers, R. R., Eberth, D. A., Fiorillo, A. R. (Eds.), *Bonebeds. Genesis,*  
948 *Analysis, and Paleobiological Significance*. The University of Chicago Press, pp.  
949 265–332.
- 950 Enloe, J. G., 2006. Geological processes and site structure: assessing integrity at a Late  
951 Paleolithic open-air site in northern France. *Geoarchaeology* 21 (6), 523–540.
- 952 Eren, M. I., Durant, A., Neudorf, C., Haslam, M., Shipton, C., Bora, J., Korisettar,  
953 R., Petraglia, M., 2010. Experimental examination of animal trampling effects on  
954 artifact movement in dry and water saturated substrates: a test case from South India.  
955 *Journal of Archaeological Science* 37 (12), 3010–3021.

- 956 Fernández-López, S. R., 1991. Taphonomic concepts for a theoretical biochronology.  
957 Revista Española de Paleontología 6, 37–49.
- 958 Fiorillo, A. R., 1991. Taphonomy and depositional setting of Careless Creek Quarry  
959 (Judith River Formation), Wheatland County, Montana, U.S.A. Palaeogeography,  
960 Palaeoclimatology, Palaeoecology 81 (3), 281–311.
- 961 García-Moreno, A., Smith, G. M., Kindler, L., Pop, E., Roebroeks, W., Gaudzinski-  
962 Windheuser, S., Klinkenberg, V., 2016. Evaluating the incidence of hydrological  
963 processes during site formation through orientation analysis. A case study of the  
964 middle Palaeolithic Lakeland site of Neumark-Nord 2 (Germany). Journal of Ar-  
965 chaeological Science: Reports 6, 82–93.
- 966 Giusti, D., Arzarello, M., 2016. The need for a taphonomic perspective in spatial analy-  
967 sis: Formation processes at the Early Pleistocene site of Pirro Nord (P13), Apricena,  
968 Italy. Journal of Archaeological Science: Reports 8, 235–249.
- 969 Harvati, K., Panagopoulou, E., Tourloukis, V., Thompson, N., Karkanas, P., Athanasi-  
970 siou, A., Konidaris, G., Tsartsidou, G., Giusti, D., 2016. New Middle Pleistocene  
971 elephant butchering site from Greece. In: Paleoanthropology Society Meeting. At-  
972 lanta, Georgia, pp. A14–A15.
- 973 Hivernel, F., Hodder, I., 1984. Analysis of artifact distribution at Ngenyem (Kenya):  
974 depositional and postdepositional effects. In: Hietala, H., Larson, P. (Eds.), Intrasite  
975 Spatial Analysis in Archaeology. Cambridge University Press, Ch. 7, pp. 97–115.
- 976 Hodder, I., Orton, C., 1976. Spatial Analysis in Archaeology. New Studies in Archae-  
977 ology. Cambridge University Press, Cambridge.
- 978 Hovers, E., Ekshtain, R., Greenbaum, N., Malinsky-Buller, A., Nir, N., Yeshurun, R.,  
979 2014. Islands in a stream? Reconstructing site formation processes in the late Middle  
980 Paleolithic site of 'Ein Qashish, northern Israel. Quaternary International 331, 216–  
981 233.
- 982 Isaac, G. L., 1967. Towards the interpretation of occupation debris: Some experiments  
983 and observations. Kroeber Anthropological Society Papers 37 (37), 31–57.
- 984 Jammalamadaka, S., Sengupta, A., Sengupta, A., 2001. Topics in Circular Statistics.  
985 Series on multivariate analysis. World Scientific.
- 986 Karkanas, P., Tourloukis, V., Thompson, N., Giusti, D., Panagopoulou, E., Harvati, K.,  
987 this issue. Sedimentology and micromorphology of the Lower Palaeolithic lakeshore  
988 site Marathousa 1, Megalopolis basin, Greece. Quaternary International.
- 989 Kluskens, S. L., 1990. Orientation and density analysis of stone artefacts at Combe-  
990 Capelle Bas, Périgord, France. Master's thesis, University of Pennsylvania.
- 991 Konidaris, G., Athanassiou, A., Tourloukis, V., Thompson, N., Giusti, D.,  
992 Panagopoulou, E., Harvati, K., this issue. The skeleton of a straight-tusked elephant

- 993 (Palaeoloxodon antiquus) and other large mammals from the Middle Pleistocene lo-  
994 cality Marathousa 1 (Megalopolis Basin, Greece): preliminary results. Quaternary  
995 International.
- 996 Krumbein, W. C., 1941. Measurement and geological significance of shape and round-  
997 ness of sedimentary particles. Journal of Sedimentary Research 11 (2), 64–72.
- 998 Lenoble, A., Bertran, P., 2004. Fabric of Palaeolithic levels: methods and implications  
999 for site formation processes. Journal of Archaeological Science 31 (4), 457–469.
- 1000 Lenoble, A., Bertran, P., Lacrampe, F., 2008. Solifluction-induced modifications  
1001 of archaeological levels: simulation based on experimental data from a modern  
1002 periglacial slope and application to French Palaeolithic sites. Journal of Archaeo-  
1003 logical Science 35 (1), 99–110.
- 1004 Lindsay, J. F., 1968. The development of clast fabric in mudflows. Journal of Sedimen-  
1005 tary Research 38 (4), 1242–1253.
- 1006 Macdonald, D. I. M., Jefferson, T. H., 1985. Orientation studies of waterlogged wood;  
1007 a paleocurrent indicator? Journal of Sedimentary Research 55 (2), 235–239.
- 1008 Malinsky-Buller, A., Hovers, E., Marder, O., 2011. Making time: ‘Living floors’,  
1009 ‘palimpsests’ and site formation processes – A perspective from the open-air Lower  
1010 Paleolithic site of Revadim Quarry, Israel. Journal of Anthropological Archaeology  
1011 30 (2), 89–101.
- 1012 Marwick, B., 2017. Computational reproducibility in archaeological research: Ba-  
1013 sic principles and a case study of their implementation. Journal of Archaeological  
1014 Method and Theory 24 (2), 424–450.
- 1015 Marwick, B., d’Alpoim Guedes, J., Barton, C. M., Bates, L. A., Baxter, M., Beavan,  
1016 A., Bollwerk, E. A., Bocinsky, R. K., Brughams, T., Carter, A. K., Conrad, C.,  
1017 Contreras, D. A., Costa, S., Crema, E. R., Daggett, A., Davies, B., Drake, B. L.,  
1018 Dye, T. S., France, P., Fullager, R., Giusti, D., Graham, S., Harris, M. D., Hawks, J.,  
1019 Heath, S., Huffer, D., Kansa, E. C., Kansa, S. W., Madsen, M. E., Melcher, J., Negre,  
1020 J., Neiman, F. D., Opitz, R., Orton, D. C., Przystupa, P., Raviele, M., Riel-Salvatore,  
1021 J., Riris, P., Romanowska, I., Smith, J., Strupler, N., Ullah, I. I., Vlack, H. G. V.,  
1022 VanValkenberg, N., Watrall, E. C., Webster, C., Wells, J., Winters, J., Wren, C. D.,  
1023 2017. Open science in archaeology. SAA Archaeological Record 17 (4), 8–14.
- 1024 McPherron, S. J., 2005. Artifact orientations and site formation processes from total  
1025 station proveniences. Journal of Archaeological Science 32 (7), 1003–1014.
- 1026 McPherron, S. J., Dibble, H. L., Goldberg, P., 2005. Z. Geoarchaeology 20 (3), 243–  
1027 262.
- 1028 Morton, A. G. T., 2004. Archaeological Site Formation: Understanding Lake Margin  
1029 Contexts. Vol. 1211 of International Series. British Archaeological Reports, Oxford.

- 1030 Nickel, B., Riegel, W., Schonherr, T., Velitzelos, E., 1996. Environments of coal forma-  
 1031 tion in the Pleistocene lignite at Megalopolis, Peloponnesus (Greece) - reconstruc-  
 1032 tion from palynological and petrological investigations. *N. Jb. Geol. Palaont. A.* 200,  
 1033 201–220.
- 1034 Ohser, J., 1983. On estimators for the reduced second moment measure of point pro-  
 1035 cesses. *Mathematische Operationsforschung und Statistik, series Statistics* 14, 63–  
 1036 71.
- 1037 Organista, E., Domínguez-Rodrigo, M., Yravedra, J., Uribe Larrea, D., Arriaza, M. C.,  
 1038 Ortega, M. C., Mabulla, A., Gidna, A., Baquedano, E., 2017. Biotic and abiotic pro-  
 1039 cesses affecting the formation of BK Level 4c (Bed II, Olduvai Gorge) and their bear-  
 1040 ing on hominin behavior at the site. *Palaeogeography, Palaeoclimatology, Palaeo-  
 1041 ecology* (in press).
- 1042 Orton, C., 1982. Stochastic process and archaeological mechanism in spatial analysis.  
 1043 *Journal of Archaeological Science* 9 (1), 1–23.
- 1044 Panagopoulou, E., Tourloukis, V., Thompson, N., Athanassiou, A., Tsartsidou, G.,  
 1045 Konidaris, G., Giusti, D., Karkanas, P., Harvati, K., 2015. Marathousa 1: a new Mid-  
 1046 dle Pleistocene archaeological site from Greece. *Antiquity Project Gallery* 89 (343).
- 1047 Petraglia, M. D., Nash, D. T., 1987. The impact of fluvial processes on experimen-  
 1048 tal sites. In: Nash, D. T., Petraglia, M. D. (Eds.), *Natural formation processes and*  
 1049 *the archaeological record*. Vol. 352 of *International Series. British Archaeological*  
 1050 *Reports*, Oxford, pp. 108–130.
- 1051 Petraglia, M. D., Potts, R., 1994. Water Flow and the Formation of Early Pleistocene  
 1052 Artifact Sites in Olduvai Gorge, Tanzania . *Journal of Anthropological Archaeology*  
 1053 13 (3), 228–254.
- 1054 Pierson, T. C., 2005. Distinguishing between debris flows and floods from field evi-  
 1055 dence in small watersheds. *USGS Numbered Series, U.S. Geological Survey*.
- 1056 R Core Team, 2017. R: A Language and Environment for Statistical Computing. R  
 1057 Foundation for Statistical Computing, Vienna, Austria.  
 1058 URL <https://www.R-project.org/>
- 1059 Ripley, B., 1977. Modelling spatial patterns. *Journal of the Royal Statistical Society,*  
 1060 *series B* 39, 172–212.
- 1061 Ripley, B., 1988. Statistical inference for spatial processes. Cambridge University  
 1062 Press.
- 1063 Ripley, B. D., 1976. The second-order analysis of stationary point processes. *Journal*  
 1064 *of Applied Probability* 13 (2), 255–266.
- 1065 Ripley, B. D., 1981. Spatial Statistics. John Wiley and Sons, New York.
- 1066 Schick, K. D., 1984. Processes of paleolithic site formation: an experimental study.  
 1067 Ph.D. thesis, University of California, Berkeley.

- 1068 Schick, K. D., 1986. Stone Age sites in the making: experiments in the formation  
1069 and transformation of archaeological occurrences. Vol. 319 of International Series.  
1070 British Archaeological Reports, Oxford.
- 1071 Schick, K. D., 1987. Modeling the formation of Early Stone Age artifact concentra-  
1072 tions. *Journal of Human Evolution* 16, 789–807.
- 1073 Schiffer, M. B., 1972. Archaeological Context and Systemic Context. *American Antiq-*  
1074 *uity* 37 (2), 156–165.
- 1075 Schiffer, M. B., 1983. Toward the identification of formation processes. *American An-*  
1076 *tiquity* 48 (4), 675–706.
- 1077 Schiffer, M. B., 1987. Formation processes of the archaeological record. University of  
1078 New Mexico Press, Albuquerque.
- 1079 Shackley, M. L., 1978. The behaviour of artefacts as sedimentary particles in a fluvialite  
1080 environment. *Archaeometry* 20 (1), 55–61.
- 1081 Sánchez-Romero, L., Benito-Calvo, A., Pérez-González, A., Santonja, M., 12 2016.  
1082 Assessment of Accumulation Processes at the Middle Pleistocene Site of Ambrona  
1083 (Soria, Spain). Density and Orientation Patterns in Spatial Datasets Derived from  
1084 Excavations Conducted from the 1960s to the Present. *PLOS ONE* 11 (12), 1–27.
- 1085 Texier, J.-P., 2000. A propos des processus de formation des sites préhistoriques / About  
1086 prehistoric site formation processes. *Paléo* 12 (1), 379–386.
- 1087 Toots, H., 1965. Orientation and distribution of fossils as environmental indicators. In:  
1088 Nineteenth Field Conference of the Wyoming Geological Association. pp. 219–292.
- 1089 Tourloukis, V., Thompson, N., Panagopoulou, E., Giusti, D., Konidaris, G., Karkanas,  
1090 P., Harvati, K., this issue. Lithic and osseous artifacts from the Lower Palaeolithic  
1091 site of Marathousa 1, Megalopolis, Greece: preliminary results. *Quaternary Interna-*  
1092 *tional*.
- 1093 van Vugt, N., de Bruijn, H., van Kolfschoten, M., Langereis, C. G., 2000. Magneto-  
1094 and cyclostratigraphy and mammal-fauna's of the Pleistocene lacustrine Megalopo-  
1095 lis Basin, Peloponnesos, Greece. *Geologica Ultrajectina* 189, 69–92.
- 1096 Vaquero, M., Chacón, M. G., García-Antón, M. D., de Soler, B. G., Martínez, K.,  
1097 Cuartero, F., 2012. Time and space in the formation of lithic assemblages: The  
1098 example of Abric Romaní Level J. *Quaternary International* 247 (0), 162–181.
- 1099 Villa, P., 2004. Taphonomy and stratigraphy in european prehistory. *Before Farming*  
1100 2004 (1), 1–20.
- 1101 Voorhies, M., 1969. Taphonomy and population dynamics of an early Pliocene ver-  
1102 tebrate fauna, Knox County, Nebraska. *Contributions to Geology, University of*  
1103 *Wyoming Special Paper* 1, 1–69.

- 1104 Walter, M. J., Trauth, M. H., 2013. A MATLAB based orientation analysis of  
1105 Acheulean handaxe accumulations in Olorgesailie and Kariandusi, Kenya Rift. Journal  
1106 of Human Evolution 64 (6), 569–581.
- 1107 Wood, R. W., Johnson, D. L., 1978. A survey of disturbance processes in archaeological  
1108 site formation. In: Schiffer, M. B. (Ed.), Advances in archaeological method and  
1109 theory. Vol. 1. Academic Press, Ch. 9, pp. 315–381.
- 1110 Woodcock, N., Naylor, M., 1983. Randomness testing in three-dimensional orientation  
1111 data. Journal of Structural Geology 5 (5), 539–548.